Supporting Information

Incorporating Functionalized Cellulose to Increase the Toughness of Covalent Adaptable Networks

JEREMY L. SWARTZ, REBECCA L. LI, AND WILLIAM R. DICHTEL*

Department of Chemistry, Northwestern University,
2145 Sheridan Rd., Evanston, Illinois 60208, USA

Correspondence Address
Professor William R. Dichtel
Department of Chemistry
Northwestern University
2045 Sheridan Road
Evanston, IL 60208 (USA)
wdichtel@northwestern.edu

Table of Contents

Materials and Instrumentation

Materials. All reagents were purchased from Sigma-Aldrich or Fisher Scientific. All reagents were used without further purification unless otherwise specified. Dimethylformamide (DMF) was purchased from Fisher Scientific and purified using a custom-built alumina-column based solvent purification system. Other solvents were purchased from Fisher Scientific and used without further purification.

Instrumentation. Infrared spectra were recorded on a Thermo Nicolet iS10 equipped with a ZnSe ATR attachment. Spectra were uncorrected.

Solution-phase NMR spectra were recorded on a Varian 400 MHz or an Agilent DD MR-400 400 MHz spectrometer using a standard 1H/X Z-PFG probe at ambient temperature.

Differential scanning calorimetry (DSC) was performed on a TA instruments Q1000 Differential Scanning Calorimeter. Samples were heated at a rate of 10 °C/min to at least 90 °C to erase thermal history, cooled to – 30 °C at 10 °C/min, and then heated to at least 120 °C. All data shown are taken from the second heating ramp. The glass transition temperature (Tg) was calculated from the maximum value of the derivative of heat flow with respect to temperature.

Dynamic mechanical thermal analysis (DMTA) was performed on a TA Instruments RSA-G2 analyzer (New Castle, DE) using rectangular films (*ca.* 1.0 mm (T) × 3 mm (W) × 6 mm (L)). The transducer was set to spring mode. The axial force was adjusted to 20 g (sensitivity 1.0 g) before the test to ensure the sample was in tension and not buckling. The minimum axial force was set to 5 g, and a force tracking mode was set such that the axial force was twice the magnitude of the oscillation force during the test. A strain adjust of 30% was set with a minimum strain of 0.05%, a maximum strain of 10%, a minimum force of 1 g and a maximum force of 20 g in order to prevent the sample from going out of the specified strain. A temperature ramp was then performed from – 30 °C to 120 °C at a rate of 5 °C/min, with an oscillating strain of 0.05% and an angular frequency of 6.28 rad s-1 (1 Hz). The glass transition temperature (T_g) was calculated from the maximum value of the loss modulus ($E``$).

Uniaxial tensile testing was conducted using dog bone shaped tensile bars (*ASTM D-1708* 1.0 mm (T) × 5 mm (W) × 25 mm (L) and a gauge length of 16 mm). The samples were aged for at least 48 h at ambient temperatures in a desiccator prior to testing. Tensile measurements were performed on a Sintech 20G tensile tester with 250 gram capacity load cell at ambient temperatures at a uniaxial extension rate of 5 mm/min. Young's modulus (E) values were calculated using the TestWorks software by taking the slope of the stress-strain curve from 0 to 1 N of force applied. Reported values are the averages and standard deviations of at least three replicates.

Stress relaxation analysis (SRA) was performed on a TA Instruments RSA-III analyzer (New Castle, DE) using rectangular films (*ca.* 1.0 mm (T) × 3 mm (W) × 20 mm (L) and a Gauge length of 6 mm). The SRA experiments were performed with strain control at specified temperature (150 to 180 °C). The samples were allowed to equilibrate at this temperature for approximately 10 minutes, after which the axial force was then adjusted to 0 N with a sensitivity of ±0.002 N. Each sample was then subjected to an instantaneous 5% strain. The stress decay was monitored, while maintaining a constant strain (5%), until the stress relaxation modulus had relaxed to at least 37%

($1/e$) of its initial value. This was performed three consecutive times for each sample.

To reprocess the materials, the polymer was ground into small pieces using a Cuisinart Grind Central coffee grinder and placed between two aluminum plates with a 1.0 mm thick aluminum spacer. This assembly was placed in a preheated PHI 30-ton manual compression hot press with 8-10 tons of force. All samples were reprocessed for 8 hours. The samples were then removed from the molds and placed in a vacuum oven for 2 days at 120 °C to further cure the materials. The samples were subjected to uniaxial tensile testing and dynamic mechanical thermal analysis to determine their recovery in mechanical properties.

Scanning electron microscopy was performed with a SEM Hitachi SU8030. The samples were cut into ½ cm x ½ cm squares and coated with 4 nm of osmium.

Scheme S1. Synthesis of bis(6-membered cyclic carbonate) (**4**) (bCC)
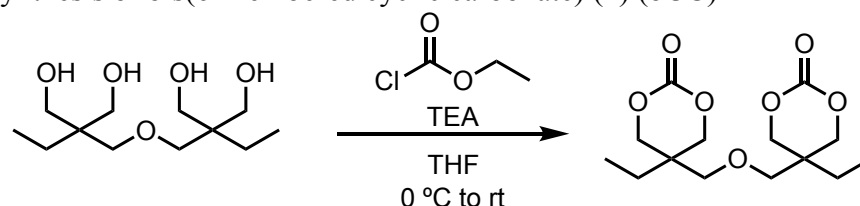
To a flame-dried round bottom flask under nitrogen, di(trimethylolpropane) (30.0 g, 120 mmol, 1 equiv.) in 700 mL of THF were added. While stirring at 0 °C, ethyl chloroformate (58.4 mL, 726 mmol, 6 equiv.) was added via syringe. Then, triethylamine (101.1 mL, 726 mmol, 6 equiv.) was added dropwise giving a white precipitate. The reaction mixture was allowed to warm to room temperature while stirring over 3 hours. The white precipitate was vacuum filtered and the filtrate was concentrated. The resulting oil was placed in the freezer to solidify. The resulting solid was recrystallized from THF (30 mL) to yield a white solid (21.5 g, 66% yield).[1]

^{1}H NMR (500 MHz, d_6-DMSO) δ 4.27 (d, J = 10 Hz, 4H, -CH_aH$_b$OCOOCH$_a$H$_b$-), 4.22 (d, J = 10 Hz, 4H, -CH$_a$H$_b$OCOOCH_aH$_b$-), 3.41 (s, 4H, -CCH_2OCH_2-), 1.39 (q, J = 7.6 Hz 4H, -CCH_2CH$_3$), 0.83 (t, J = 7.6 Hz, 6H, -CCH$_2$CH_3) ppm.

^{13}C NMR (125 MHz, d_6-DMSO): δ 148.4, 72.8, 70.6, 35.2, 23.2, 7.65 ppm.

FT-IR (solid, ATR): 2972, 2881, 1732, 1539, 1463, 1412, 1388, 1306, 1253, 1184, 1152, 1106, 1060, 1016, 988, 961, 868, 797, 762, 702 cm^{-1}

Scheme S2. Benzyl-protection of 2,2-bis(hydroxymethyl)propionic acid (S**1**)
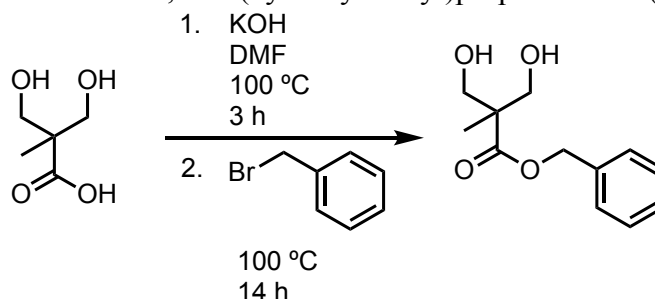
To a flame-dried round bottom flask under nitrogen, 2,2-bis(hydroxymethyl)propionic acid (65.2 g, 486 mmol, 1 equiv.) was added and dissolved in DMF (360 mL). To this, potassium hydroxide (27.5 g, 491 mmol, 1.01 equiv.) was added. The reaction was allowed to stir at 100 °C for 3 h. After 3 h, benzyl bromide (69.5 mL, 585 mmol, 1.2 equiv.) was added via syringe to give a white precipitate. This crude reaction solution was allowed to stir at 100 °C for 14 h. The precipitate was removed by vacuum filtration. The solvent was removed from the filtrate by vacuum distillation at 100 °C to yield a white solid. The solid was recrystallized from toluene (75 mL) to yield the product as a white solid (63 g, 57.8 % yield).

^{1}H NMR (500 MHz, d_6-DMSO): δ 7.34 (m, 5H, C$_6$H$_5$CH$_2$-), 5.10 (s, 2H, C$_6$H$_5$CH_2OCO-), 4.74 (t, J = 5.4 Hz, 2H, [CH$_2$OH]$_2$C-), 3.56 (dd, J = 10.4, 5.5 Hz, 2H, [OHCH_aH$_b$]$_2$C-), 3.47 (dd, J = 10.4, 5.4 Hz, 2H, [OHCH$_a$H$_b$]$_2$C-), 1.10 (s, 3H, CH_3C[CH$_2$OH]$_2$) ppm.

^{13}C NMR (125 MHz, d_6-DMSO): δ 174.5, 136.5, 128.3, 127.6, 127.1, 65.0, 63.9, 50.3, 16.9 ppm.

FT-IR (solid, ATR): 3508, 3358, 3091, 3063, 3038, 2981, 2943, 2885, 1702, 1607, 1585, 1549, 1498, 1465, 1456, 1406, 1377, 1366, 1322, 1315, 1300, 1223, 1180, 1153, 1114, 1039, 1030, 1001, 976, 946, 910, 749, 699 cm^{-1}

Scheme S3. Synthesis of benzyl-protected carboxylate-containing 6-membered cyclic carbonate (**S2**)
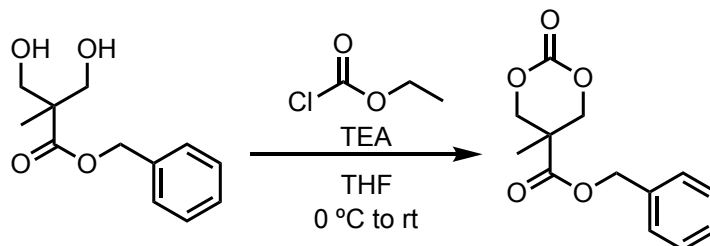

To a flame dried round bottom flask under nitrogen, **1** (30 g, 133.8 mmol, 1 equiv.) was added with THF (300 mL). The solution was cooled to 0 °C. To this, ethyl chloroformate (38.4 mL, 401.3 mmol, 3 equiv.) and triethylamine (65.8 mL, 468.2 mmol, 3.5 equiv.) were added to yield a white precipitate. The reaction was allowed to stir for 3 h and was brought to room temperature. After 3 h, the precipitate was removed via vacuum filtration. The filtrate was concentrated to yield an off-white solid. The crude solid was recrystallized from toluene to yield a white solid (25.5 g, 75 % yield).

^{1}**H NMR** (500 MHz, d_6-DMSO): δ 7.38 (m, 5H, C$_6$H$_5$CH$_2$-), 5.22 (s, 2H, C$_6$H$_5$CH$_2$OCO-), 4.60 (d, J = 10.6 Hz, 2H, -CH$_a$H$_b$OCOOCH$_a$H$_b$-), 4.39 (d, J = 10.5 Hz, 2H, -CH$_a$H$_b$OCOOCH$_a$H$_b$-), 1.21 (s, 3H, CH$_3$CCOO-) ppm.

^{13}**C NMR** (125 MHz, d_6-DMSO): δ 172.0, 147.6, 136.0, 129.0, 128.6, 128.1, 72.9, 67.2, 39.7, 16.8 ppm.

FTIR (solid, ATR): 3034, 2982, 2948, 2913, 2883, 1733, 1608, 1586, 1536, 1499, 1474, 1466, 1458, 1406, 1378, 1334, 1314, 1286, 1228, 1171, 1130, 1096, 1035, 1011, 992, 932, 767, 738, 696 cm^{-1}

Scheme S4. Synthesis of carboxylic acid-containing 6-membered cyclic carbonate (**S3**)
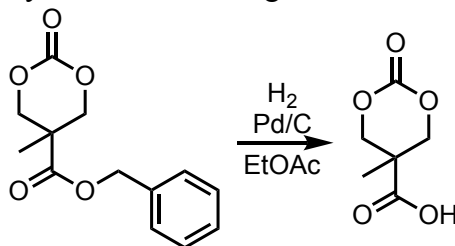
A solution of **2** (20 g, 79.9 mmol) and ethyl acetate (267 mL) was made in a round bottom flask and mixed until homogeneous. To a Parr reactor, palladium on carbon (10 wt% loading, 1.32 g) was added with a stir bar. The solution of **2** and ethyl acetate was added to the Parr reactor. The reactor was sealed and filled with H$_2$ (10 bar). The reaction was stirred at rt for 4 h at which the reactor was vented and refilled with H$_2$ (10 bar). The reaction was allowed to stir at rt for 16 h. The parr reactor was then vented and the palladium on carbon was removed via vacuum filtration on celite. The celite was washed thoroughly with ethyl acetate to remove all of the product, the solutions were combined and concentrated to yield **3** as a tan powder (11.9 g, 93.3% yield).

^{1}**H NMR** (500 MHz, d_6-DMSO): δ 13.4 (br s, 1H, -COOH), 4.54 (d, J = 10.1 Hz, 2H, -CH$_a$H$_b$OCOOCH$_a$H$_b$-), 4.31 (d, J = 10.1 Hz, 2H, -CH$_a$H$_b$OCOOCH$_a$H$_b$-), 1.17 (s, 3H, -CH$_3$CCOOH) ppm.

^{13}**C NMR** (125 MHz, d_6-DMSO): δ 173.8, 147.8, 73.2, 39.8, 16.9 ppm.

FT-IR (solid, ATR): 2988, 2624, 1744, 1694, 1537, 1464, 1418, 1372, 1311, 1282, 1241, 1199, 1176, 1138, 1102, 969, 936, 814, 799, 767, 748, 720 cm^{-1}

Scheme S5. Synthesis of acid chloride-containing 6-membered cyclic carbonate (**1**)
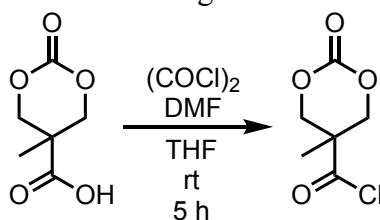

To a flame-dried round bottom flask under nitrogen, **3** (2.0 g, 12.4 mmol, 1 equiv.) was added and dissolved in anhydrous THF (62 mL). To this, oxalyl chloride (1.2 mL, 13.8 mmol, 1.1 equiv.) and DMF (20 drops) were added to the solution. The reaction was allowed to stir at room temperature for 5 h. Then the reaction mixture was concentrated and diluted with DCM and again was concentrated, resulting in a yellow oil. This oil was dried *in vacuo* to remove the excess oxalyl chloride to yield a yellow solid (**4**).

^{1}H NMR (500 MHz, d_6-DMSO): δ 4.54 (d, J = 10.5 Hz, 2H, -CH$_a$H$_b$OCOOCH$_a$H$_b$-), 4.32 (d, J = 10.4 Hz, -CH$_a$H$_b$OCOOCH$_a$H$_b$-), 1.17 (s, 3H, CH$_3$CCOCl) ppm.

^{13}C NMR (125 MHz, d_6-DMSO): δ 173.2, 147.3, 72.6, 39.3, 16.3 ppm

FT-IR (solid, ATR): 2978, 1728, 1525, 1464, 1416, 1400, 1268, 1230, 1200, 1179, 1144, 1103, 1028, 982, 931, 888, 804, 763, 736, 686 cm^{-1}
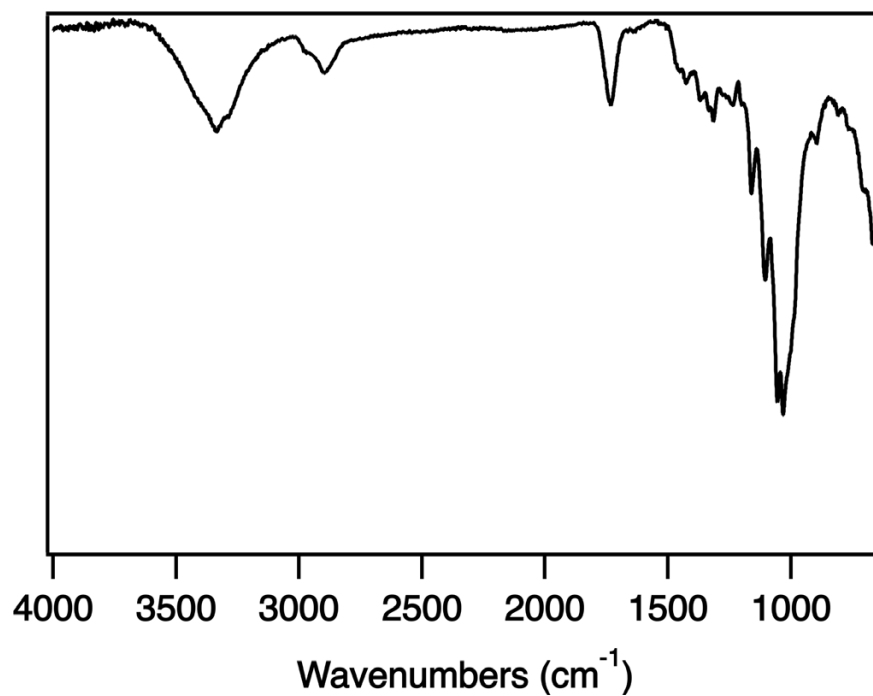
Figure S1. FTIR spectrum of **2** showing functionalization of the cellulose by cyclic carbonate **1** through the appearance of the C=O stretch at 1732 cm^{-1}.
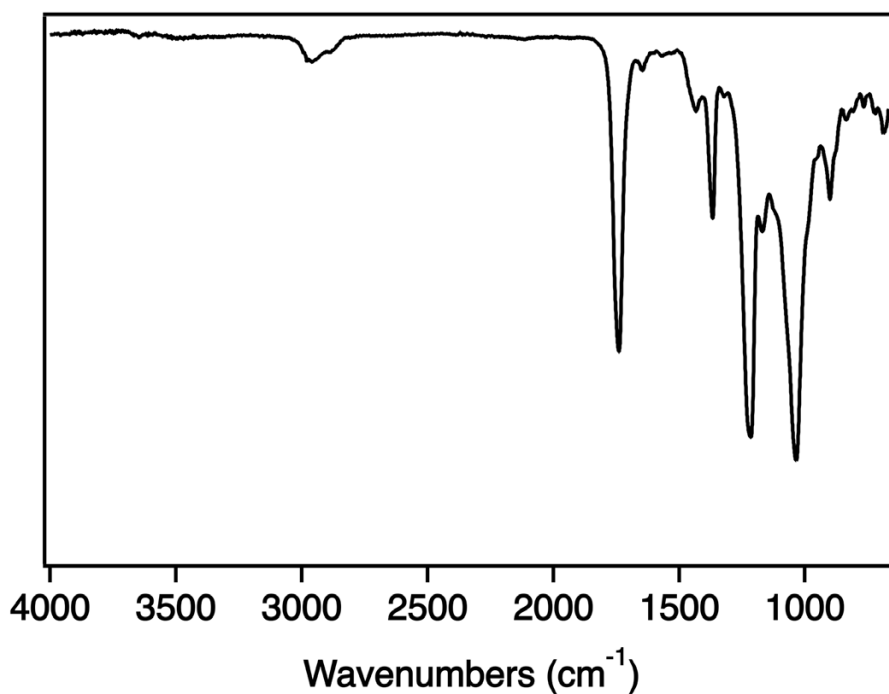
Figure S2. FTIR spectrum of **3** showing complete acylation of the hydroxyl groups on the cellulose through the loss of the O-H stretch at 3333 cm^{-1}.
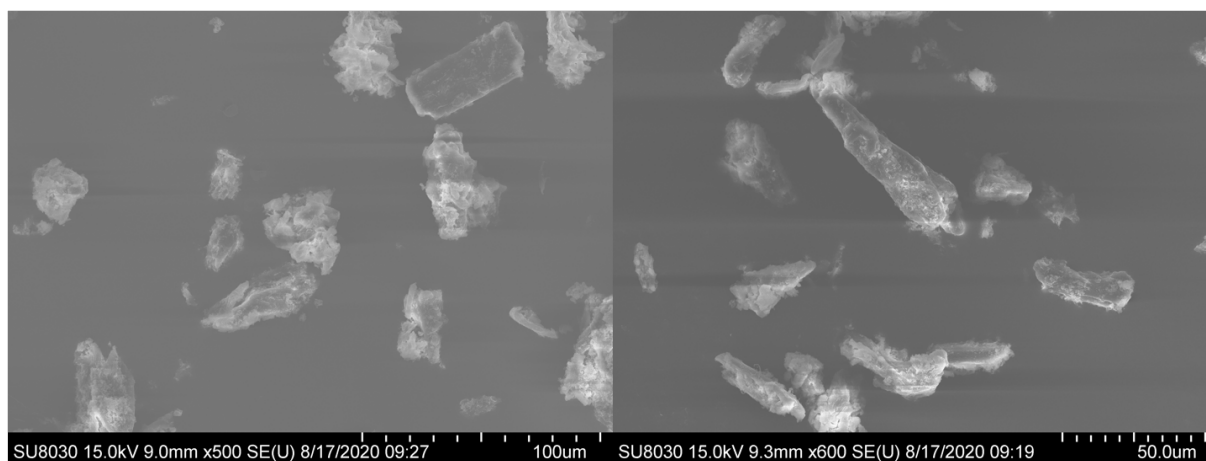
Figure S3. SEM images of the functionalized cellulose filler as a powder showing that the particles are ~3-5 microns in size.
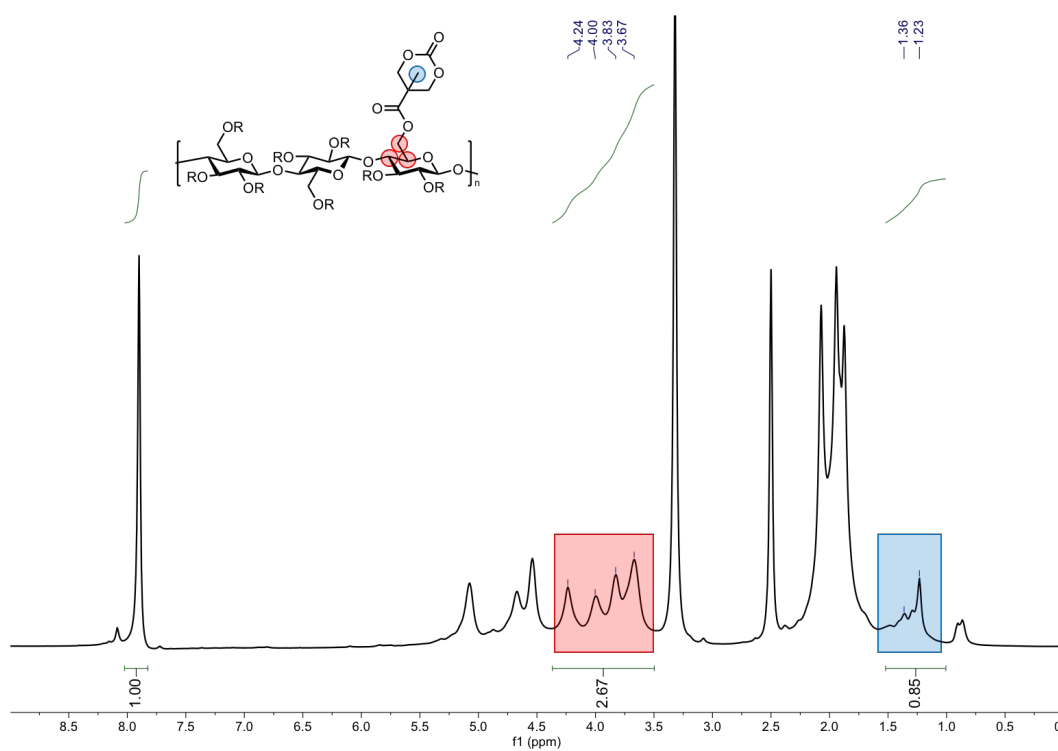
Figure S4. ¹H NMR quantification of the functionalization of cellulose with the cyclic carbonate moiety using tribromobenzene as the internal standard. Integration of the resonance at 1.23 ppm for the methyl group on the cyclic carbonate and comparing that to the integration of the peaks at 3.67-4.24 ppm for the cellulose protons labeled gives the ratio of 3 sugar monomer rings per cyclic carbonate.
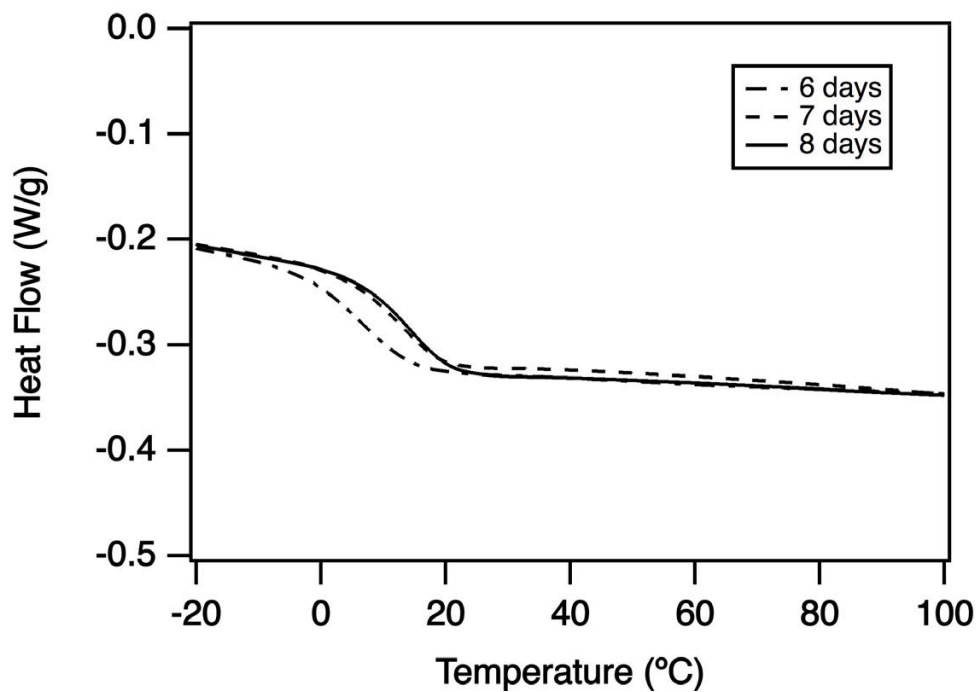
Figure S5. DSC experiment to show when control film is cured fully due to the T_g being the same after 8 days of heating at 120 °C.
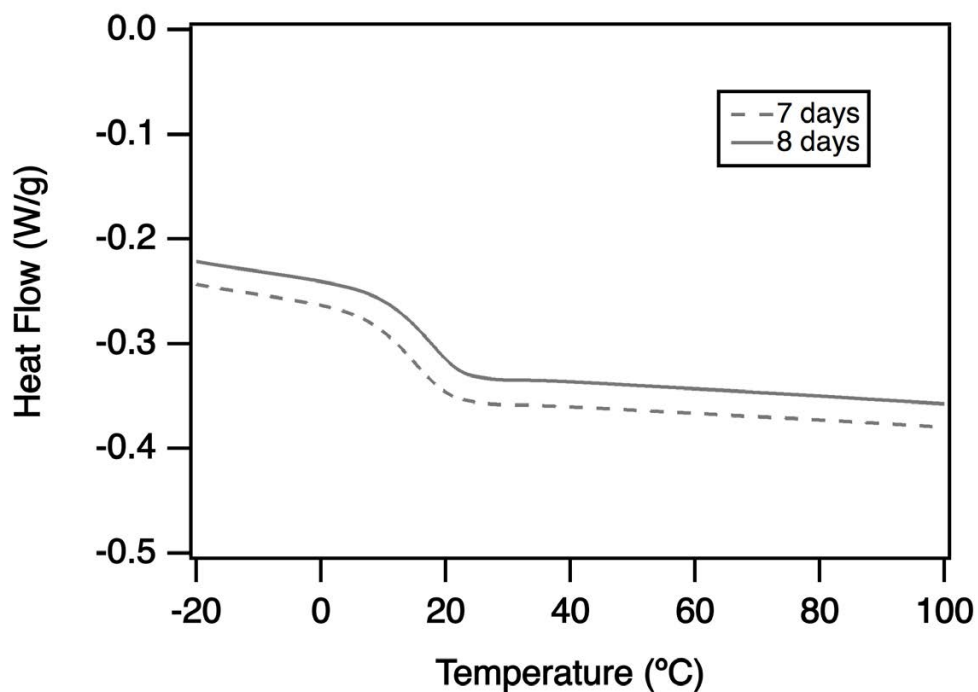
Figure S6. DSC experiment to show when 6.6 wt% film is cured fully due to the T_g being the same after 8 days of heating at 120 °C.

Table S1. Glass-transition temperatures (T_gs) and gel fractions for the control and cellulose-incorporated films. Glass-transition temperatures were determined by both differential scanning calorimetry (DSC) and dynamic mechanical thermal analysis (DMTA).

Cellulose Content in sample	$T_{g,DSC}$ (°C)	$T_{g,DMTA}$ (°C)	Gel Fraction (%)
0 wt%	12	14	83.5
1.3 wt%	12	16	82.5
2.7 wt%	17	22	74.4
4.0 wt%	17	13	84.0
5.3 wt%	8	25	88.7
6.6 wt%	17	17	80.4
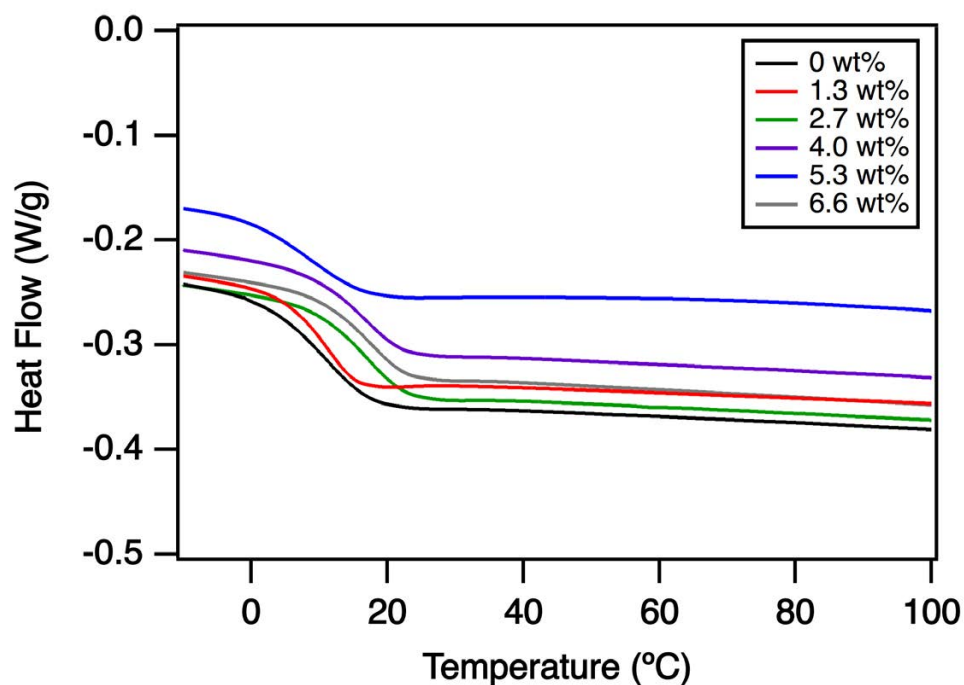
Figure S7. DSC plots of cellulose incorporated films and control showing the glass-transition temperature for each film.
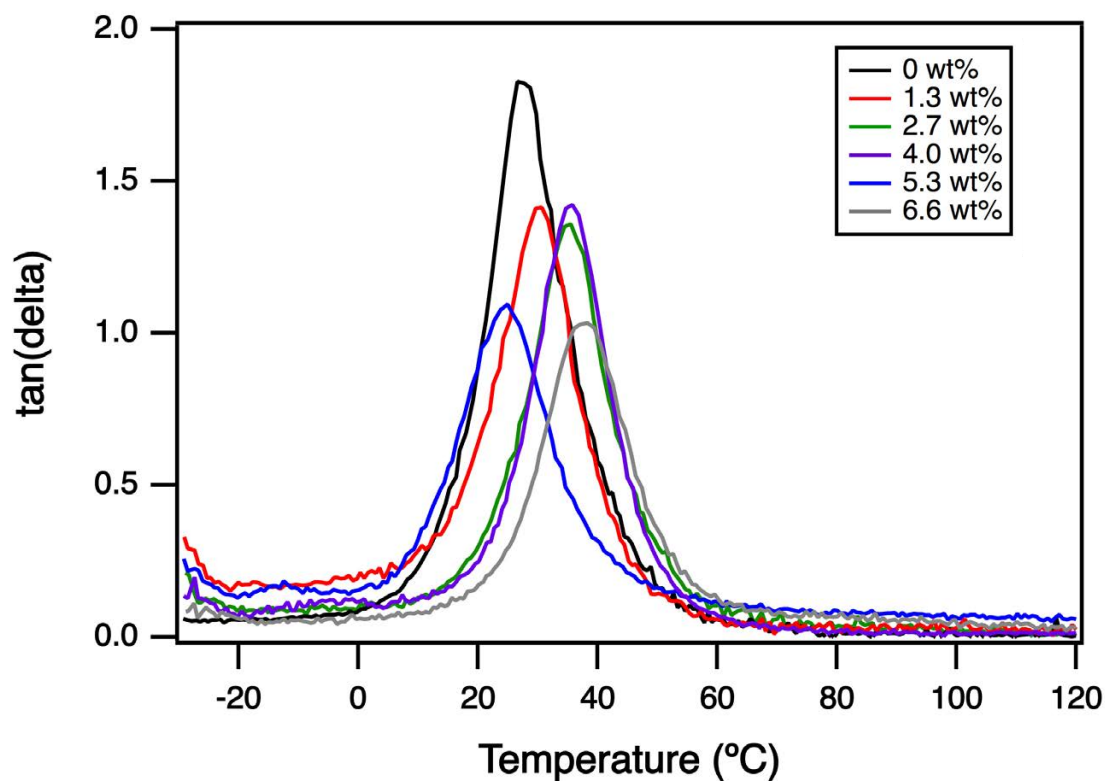
Figure S8. Tan(delta) data for the polycarbonate films showing that all of the values are above 1, which denotes that the films are homogenous.
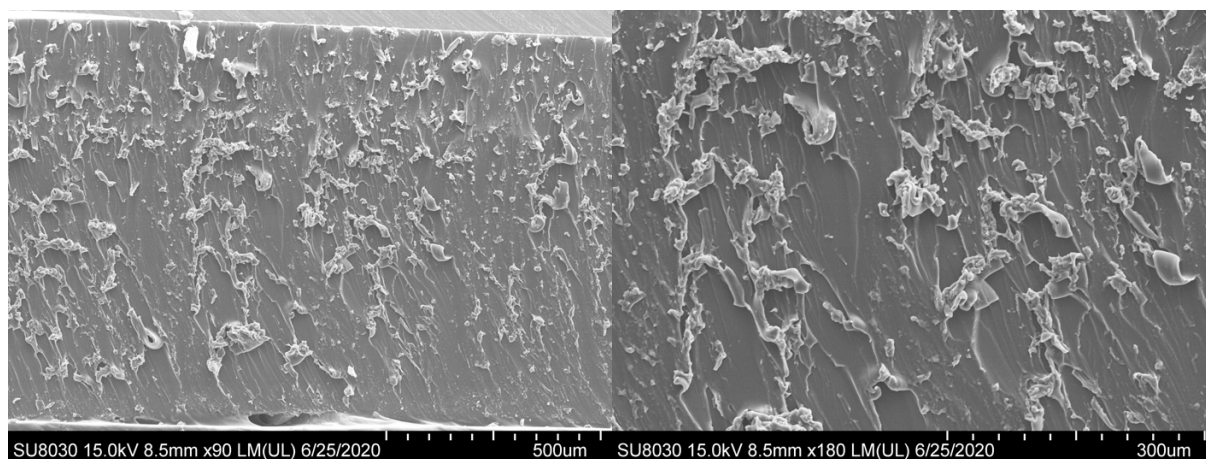
Figure S9. Cross-sectional SEM images of the unfilled as synthesized PC CAN.
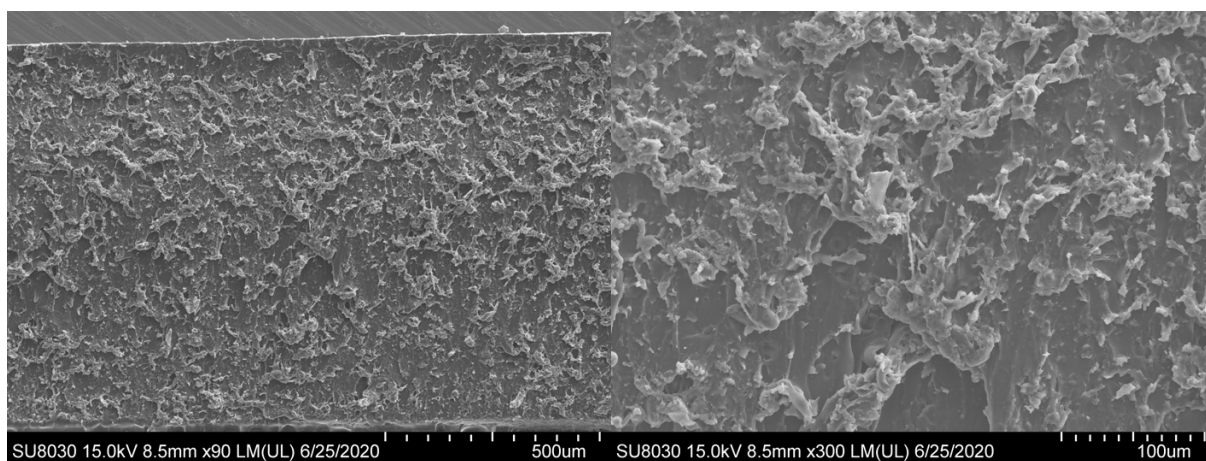
Figure S10. Cross-sectional SEM images of the 6.6 wt% as synthesized PC CAN showing that the filler is dispersed throughout and there are no aggregation events seen in the material.
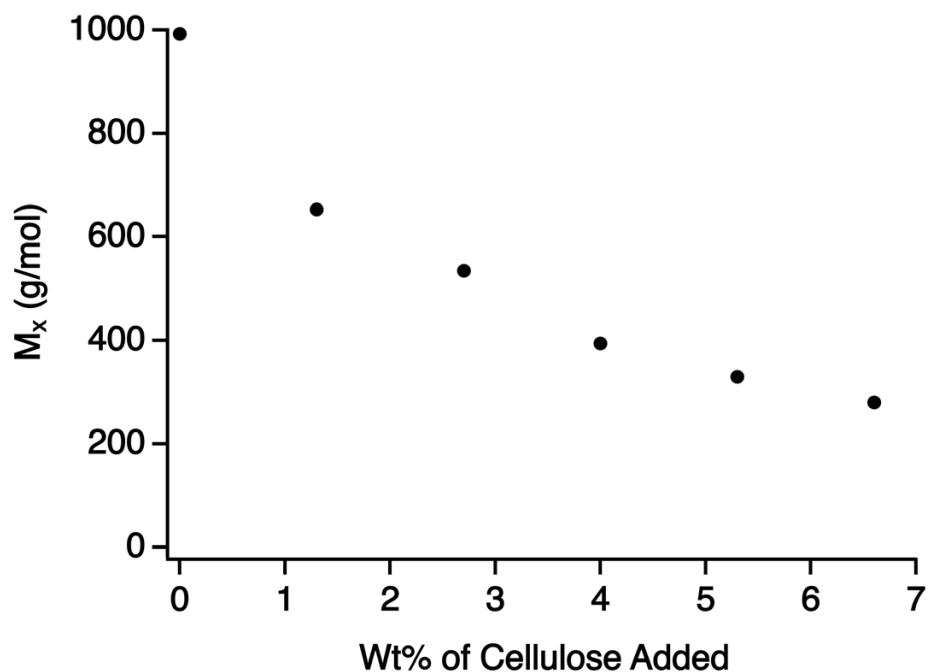
Figure S11. Plot of molecular weight between crosslinks (M_x) versus mol% cellulose incorporated. The molecular weight between crosslinks was determined from the storage modulus at 100 °C of the DMTA plot.
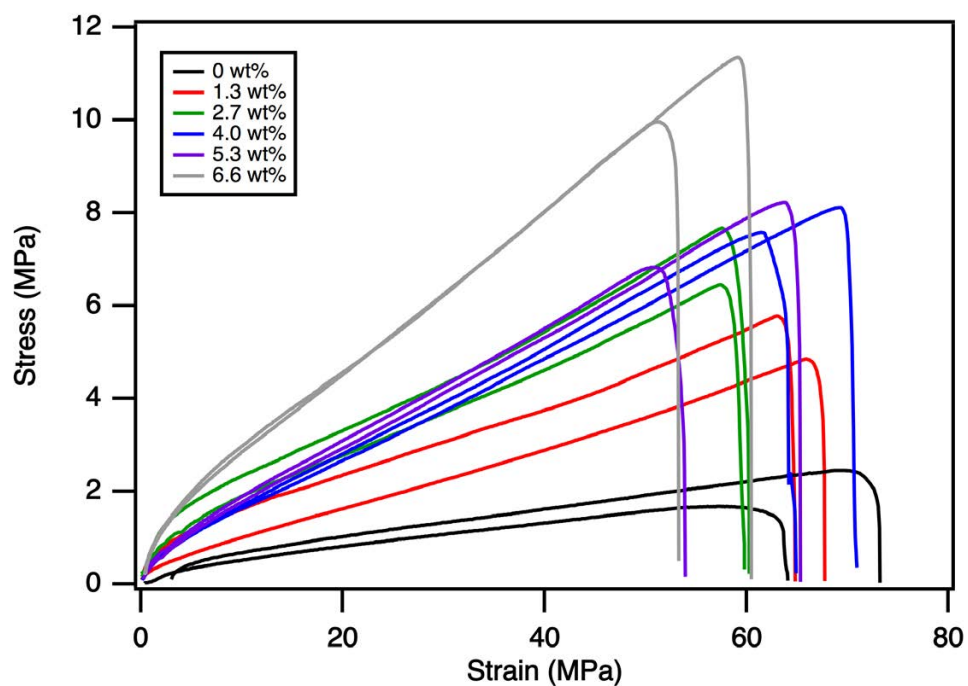
Figure S12. Stress-strain curves for multiple trials of each PC CAN sample containing differing amounts of filler.

Table S2. Tensile data for as synthesized polycarbonate films.

Sample	Tensile Stress (MPa)	Strain at Break (%)	Modulus (MPa)	Toughness (J/m^3)
0 wt%	2.3 ± 0.5	77.9 ± 19.4	8 ± 1	103 ± 34
1.3 wt%	4.9 ± 0.9	60.8 ± 6.4	111 ± 50	168 ± 43
2.7 wt%	5.6 ± 2.2	55.8 ± 2.3	50 ± 13	189 ± 71
4.0 wt%	7.1 ± 1.4	65.2 ± 5.5	181 ± 29	258 ± 56
5.3 wt%	9.5 ± 1.2	63.2 ± 13.3	148 ± 85	270 ± 56
6.6 wt%	10.2 ± 0.8	50.2 ± 6.9	424 ± 91	331 ± 42
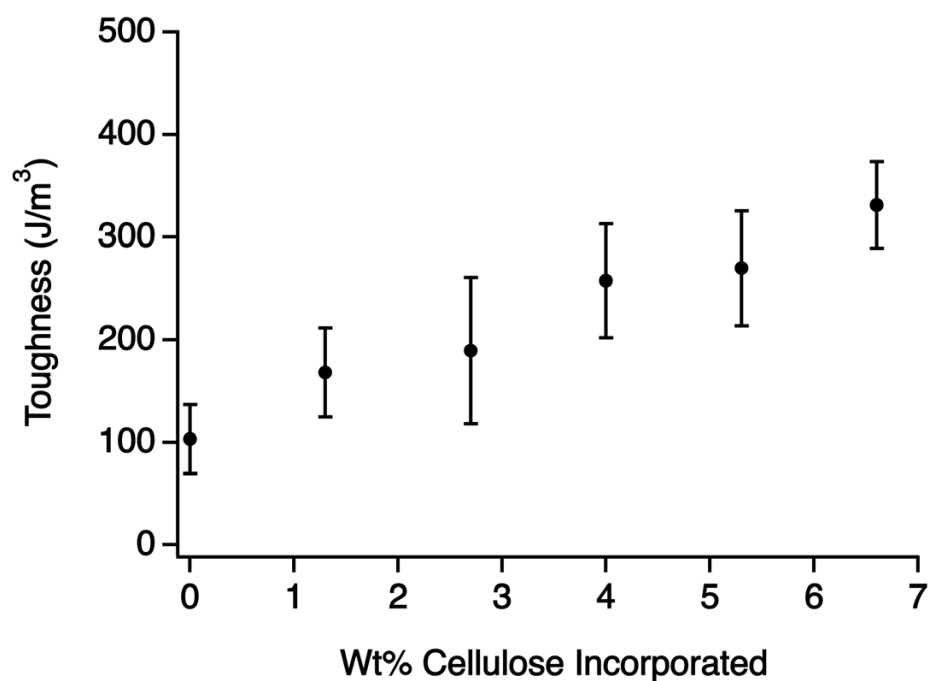
Figure S13. Plot of toughness versus mol% cellulose incorporated. The plot shows that with increasing functionalized cellulose amounts in the film, the toughness increases.
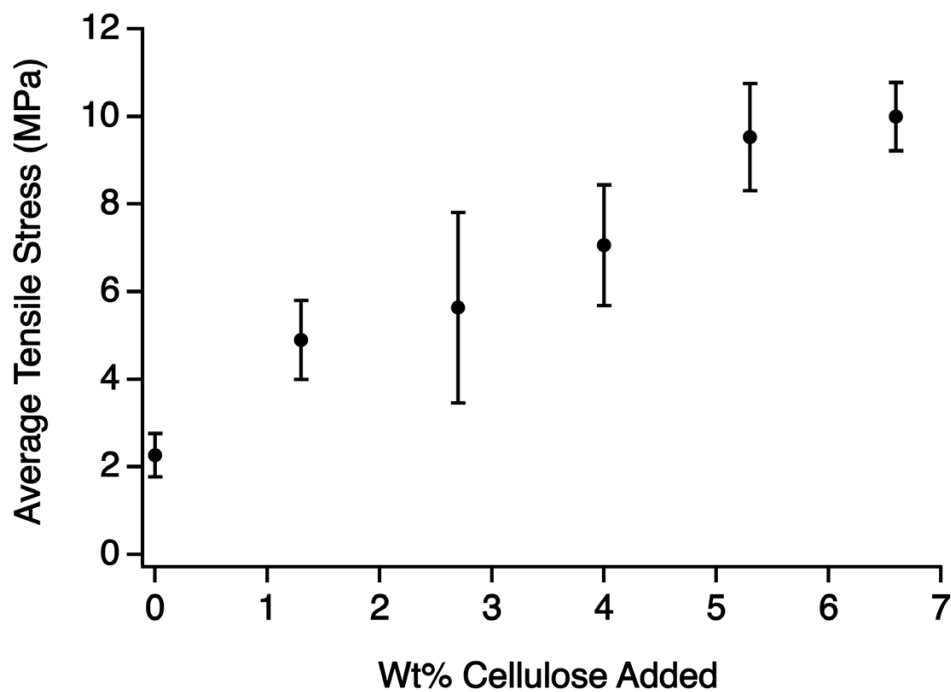
Figure S14. Plot of average tensile stress versus mol% cellulose added. The tensile stress was determined by the maximum stress of the stress-strain curve from tensile testing.
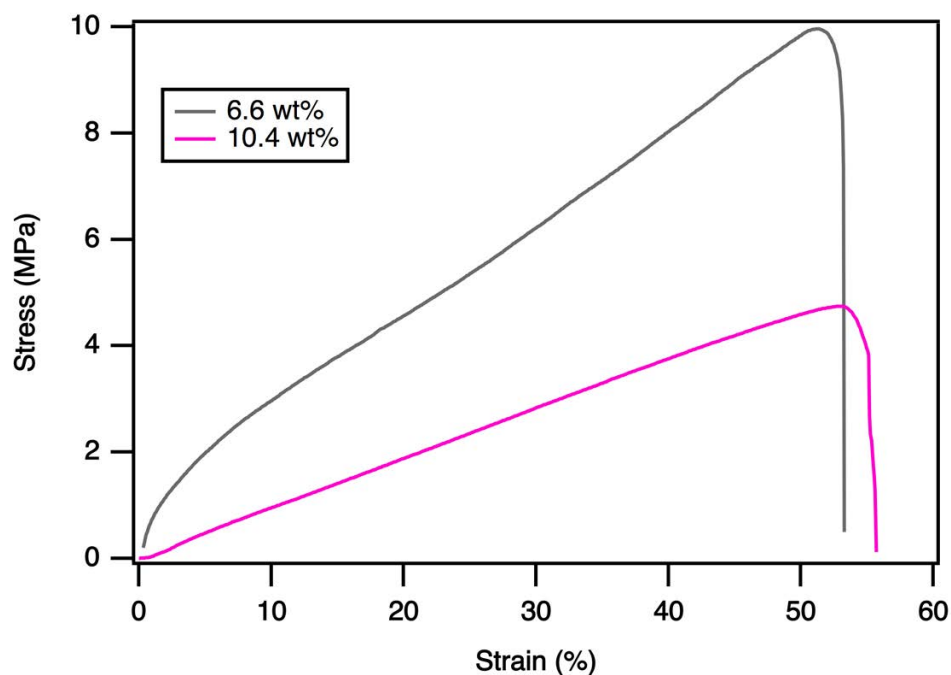
Figure S15. Tensile plot comparing the 6.6 wt% tensile properties and those of 10.4 wt% PC film. This plot shows that the mechanical enhancement from the filler incorporation is lost at loadings higher than 6.6 wt%.
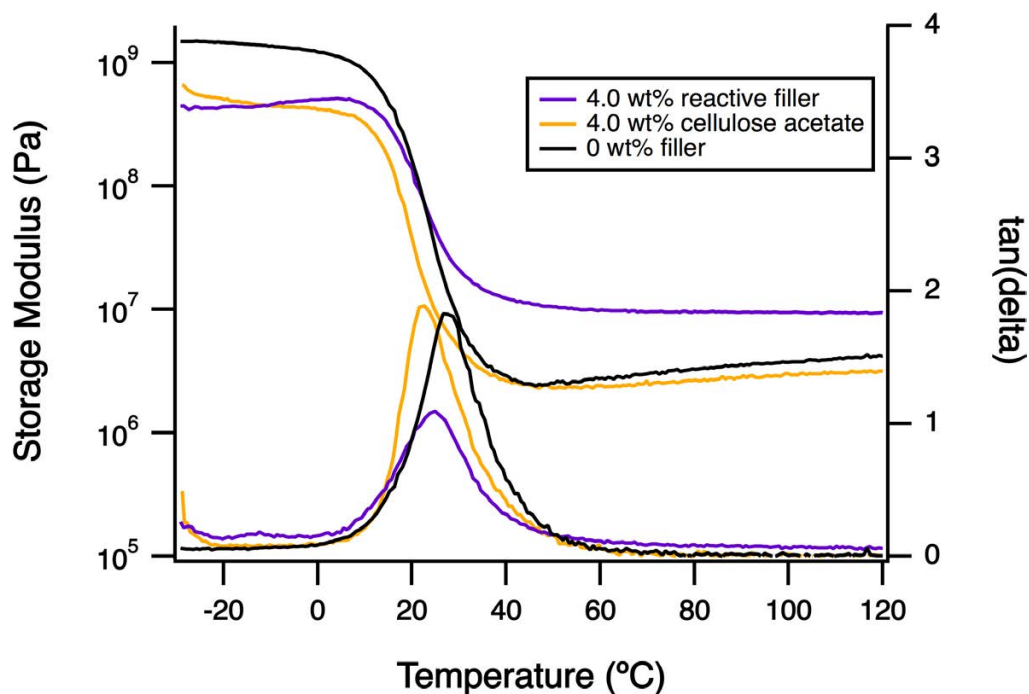
Figure S16. DMTA plot comparing the crosslinking density of the 4.0 wt% functionalized cellulose reactive filler with that of a 4.0 wt% cellulose acetate film. When comparing those two samples to the unfilled film, the sample containing cellulose acetate as the filler showed no increase in crosslinking density as the sample containing the reactive filler.
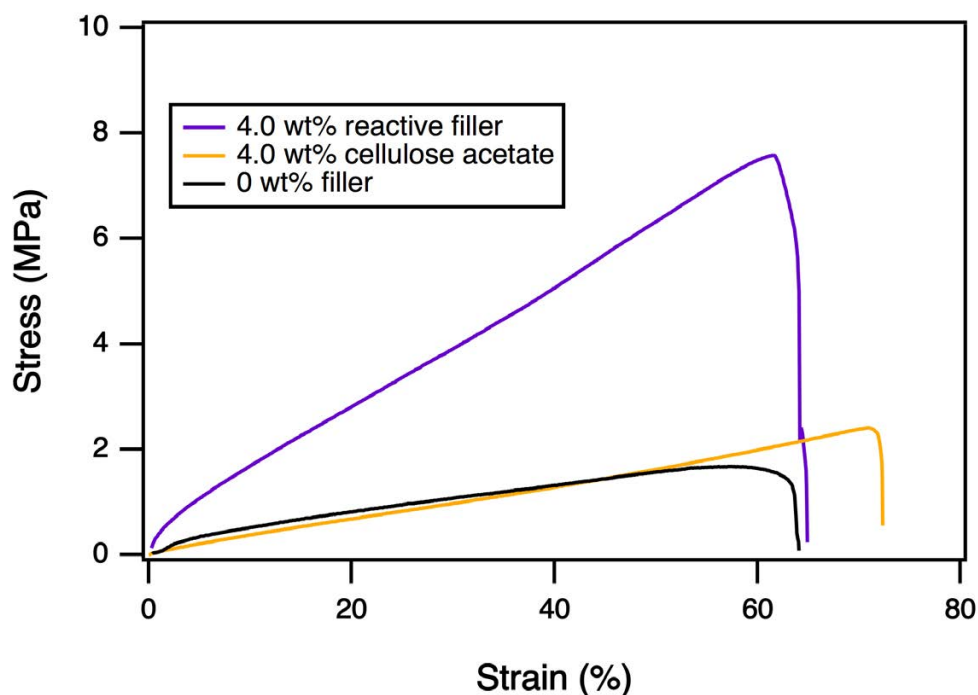
Figure S17. Tensile plot comparing the tensile properties of the films containing 4.0 wt% functionalized cellulose reactive filler to those of the 4.0 wt% cellulose acetate filler sample and the unfilled sample.

Table S3. Relaxation times (τ^*) from 160-180 °C for the polycarbonate films.

Cellulose Content in Sample (wt%)	Relaxation Times at Given Temperature (s)		
	180 °C	170 °C	160 °C
0	50	235	393
	60	225	449
	80	182	493
1.3	90	165	425
	100	200	479
	70	273	436
2.7	151	501	1395
	121	491	1676
	154	582	1368
4.0	163	464	1738
	138	626	1300
	159	491	1705
5.3	321	760	3954
	332	845	3562
	341	966	2936
6.6	354	1586	5574
	342	2070	4336
	398	2002	5515

Table S4. Activation energies for the cellulose polycarbonate films and the R^2 for the linear fit of the log (τ^*) versus 1000/T plot to determine the activation energy.

Sample	Activation Energies (E_a, kJ/mol)	R^2 of linear fit for E_a
0 wt%	69 ± 3	0.976
1.3 wt%	58 ± 1	0.995
2.7 wt%	83 ± 2	0.994
4.0 wt%	83 ± 1	0.998
5.3 wt%	84 ± 2	0.990
6.6 wt%	92 ± 4	0.974
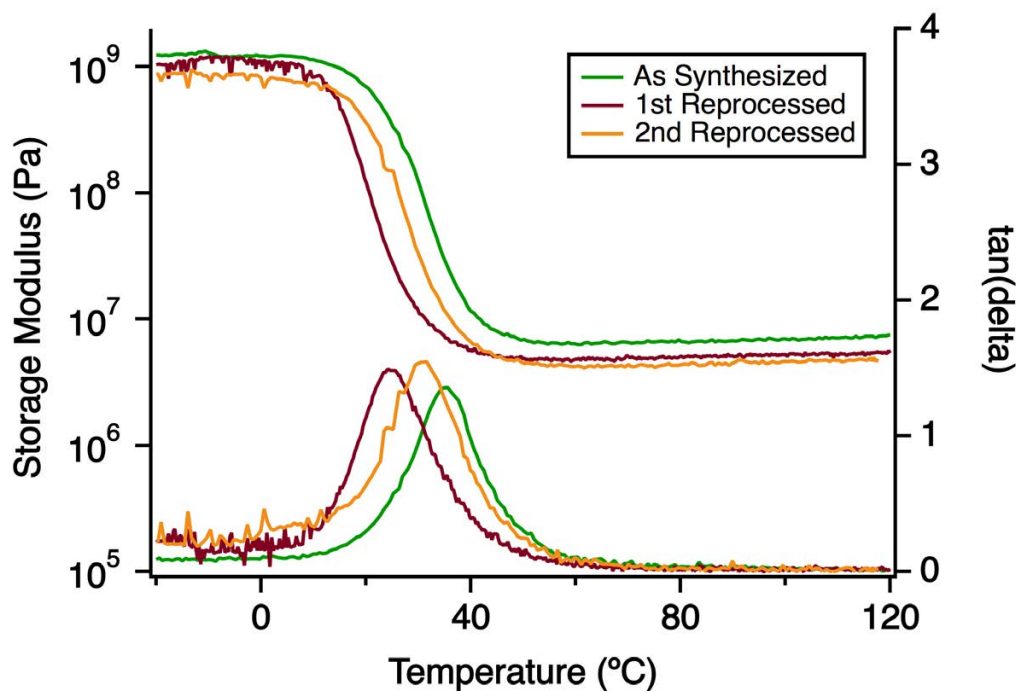
Figure S18. DMTA plot of 2.7 wt% as synthesized and reprocessed after reprocessing at 140 °C for 8 hours followed by a curing for 2 days at 120 °C, resulting in an 75% recovery in crosslink density in the reprocessed sample compared to as synthesized.
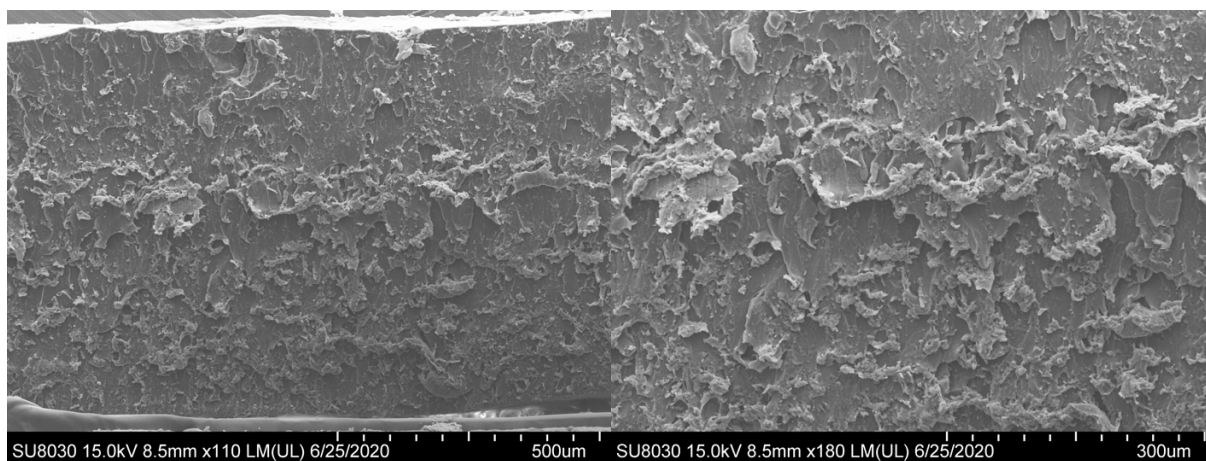
Figure S19. Cross-sectional SEM images of the reprocessed 6.6 wt% film. Possible aggregation in the material in the center of the sample.
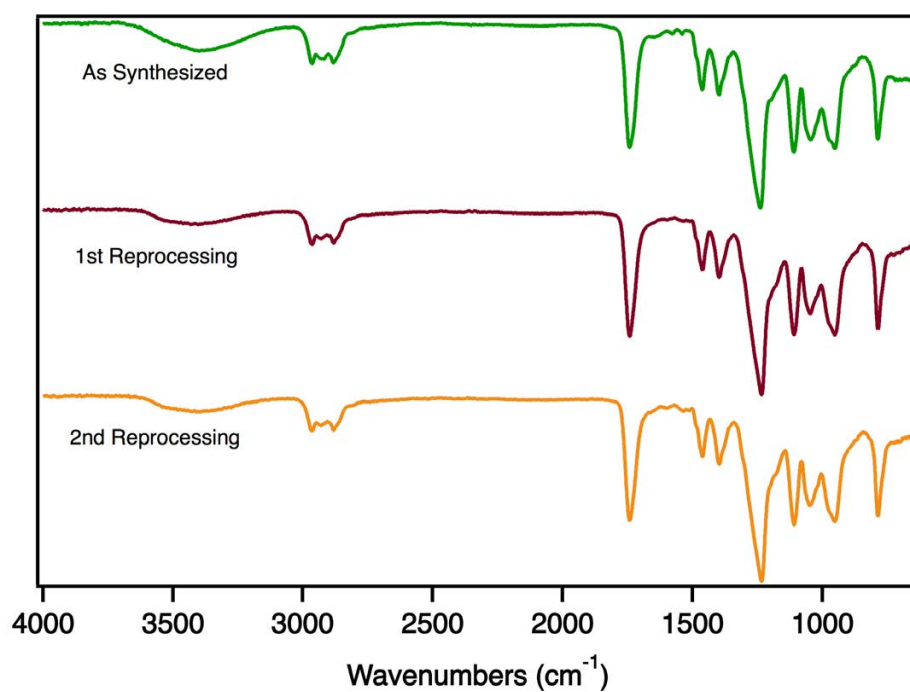

**Figure S20.** FT-IR of the 2.7 wt% as synthesized and reprocessed films.
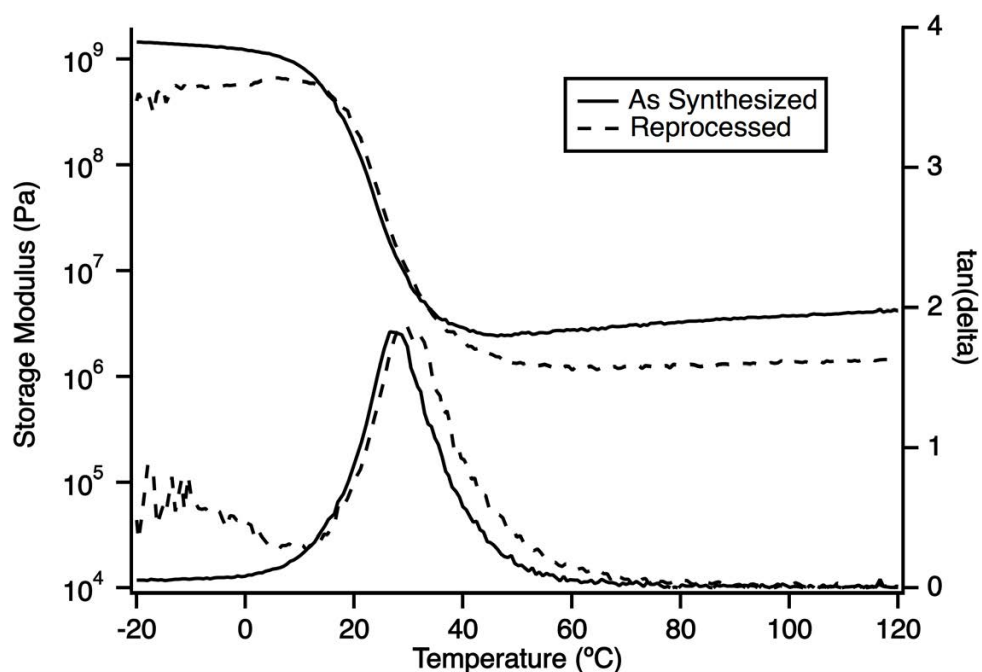
Figure S21. DMTA of as synthesized and reprocessed films showing a similar T_g after reprocessing, resulting in a 33% recovery in the crosslinking density.

Table S5. Tensile data for the reprocessed films.

Sample	Tensile Stress (MPa)	Strain at Break (%)	Modulus (MPa)	Toughness (J/m^3)
2.7 wt 1st Reprocessed	5.5 ± 0.6	49.4 ± 0.3	13.5 ± 2.1	164 ± 21
2.7 wt% 2nd Reprocessed	4.5 ± 0.2	64.5 ± 7.3	27 ± 1	200 ± 2
6.6 wt% 1st Reprocessed	8.5 ± 1.3	54.0 ± 6.8	30.7 ± 7.1	269 ± 62
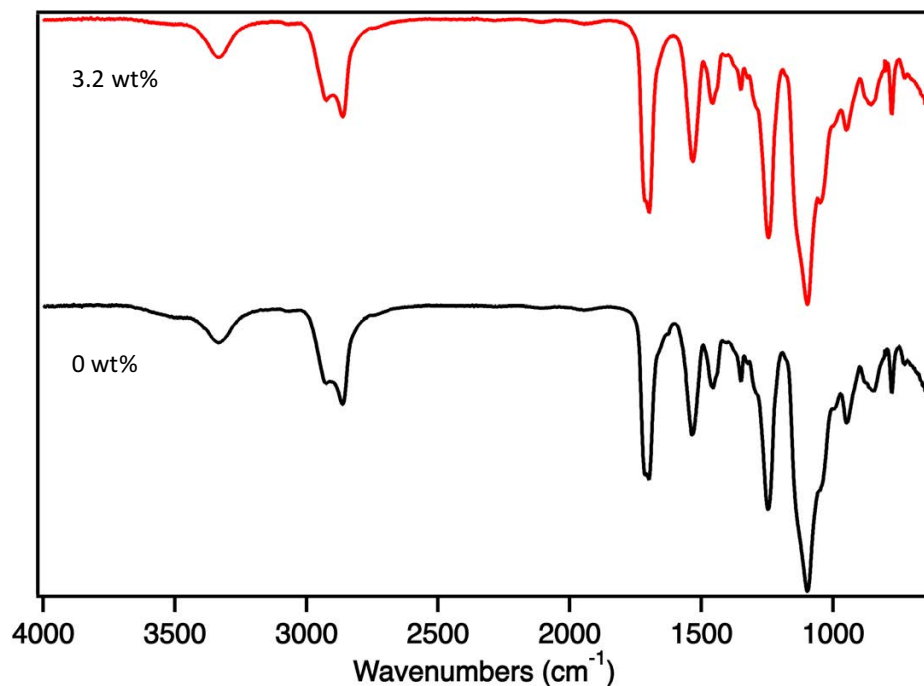
Figure S22. FT-IR of the polyurethane films showing the lack of the isocyanate stretch around 2200 cm^{-1} denoting that the films are fully cured.
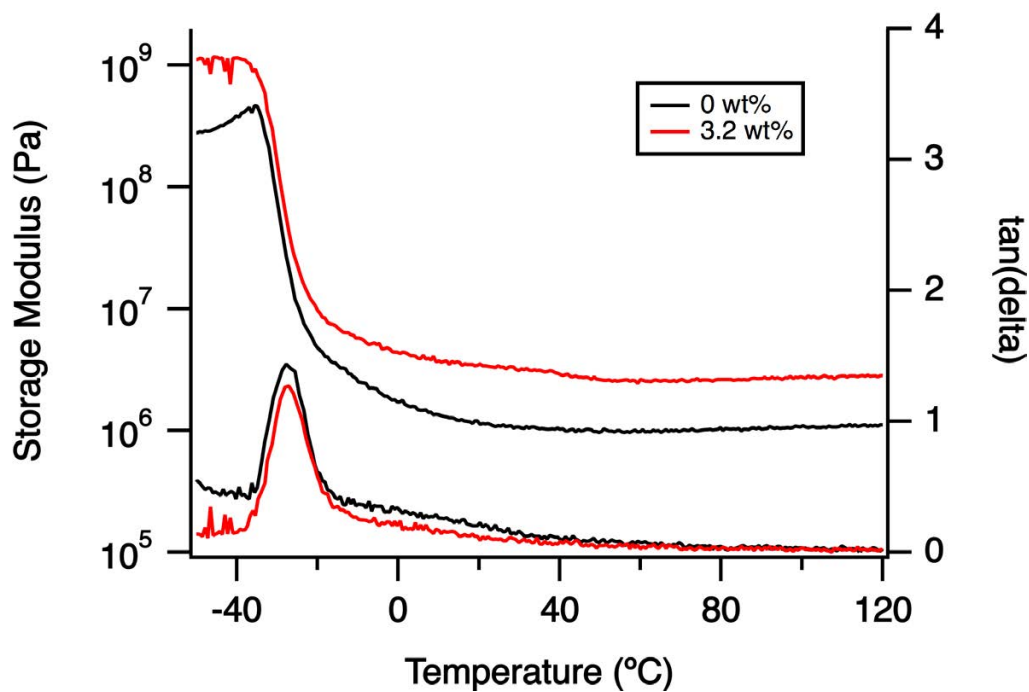
Figure S23. DMTA plots of the polyurethane films with and without the cellulose prepolymer. The crosslinking density increases 2.5x with 3.2 wt% of the cellulose prepolymer added.

Table S6. Tensile data for the polyurethane films.

Sample	Tensile Stress (MPa)	Strain at Break (%)	Modulus (MPa)	Toughness (J/m^3)
0 wt%	0.7 ± 0.3	90 ± 1	2 ± 1	61 ± 11
3.2 wt%	1.3 ± 0.4	107 ± 3	2 ± 1	143 ± 2

Table S7. Activation energies for the cellulose polyurethane films and the R^2 for the linear fit of the log (τ*) versus 1000/T plot to determine the activation energy.

Sample	Activation Energies (E_a, kJ/mol)	R^2 of linear fit for E_a
0 wt%	68 ± 3	0.976
3.2 wt%	71 ± 1	0.997
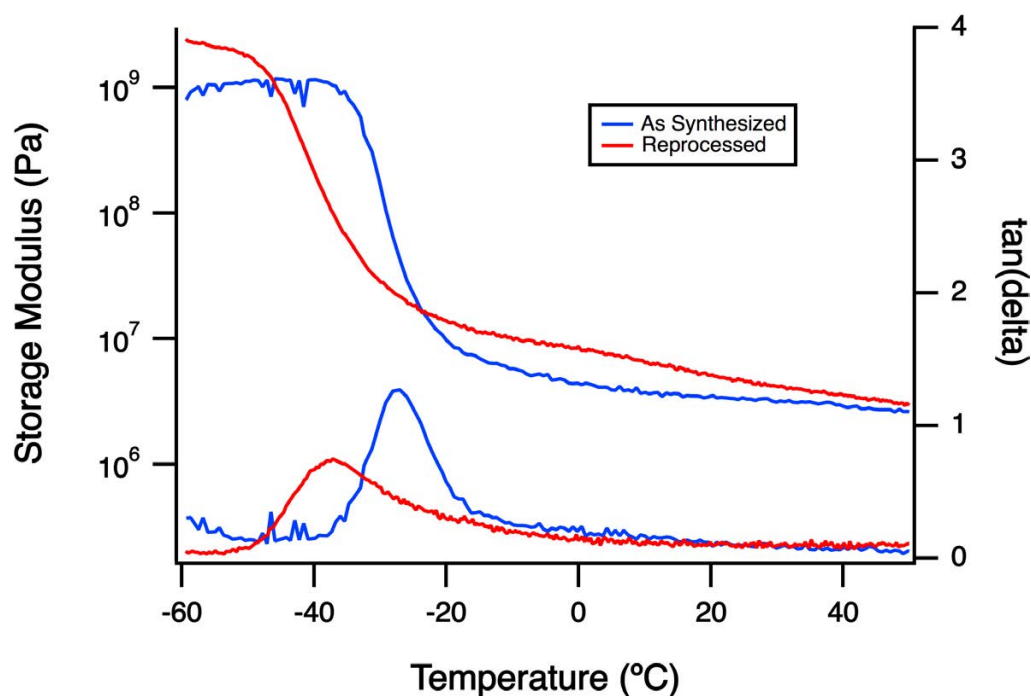
Figure S24. DMTA plot of the 3.2 wt% PU CAN before and after reprocessing at 160 °C for 1 h. The plot shows that the enhanced crosslinking density of the material can be maintained after reprocessing.

Polycarbonate Films-SRA Plots
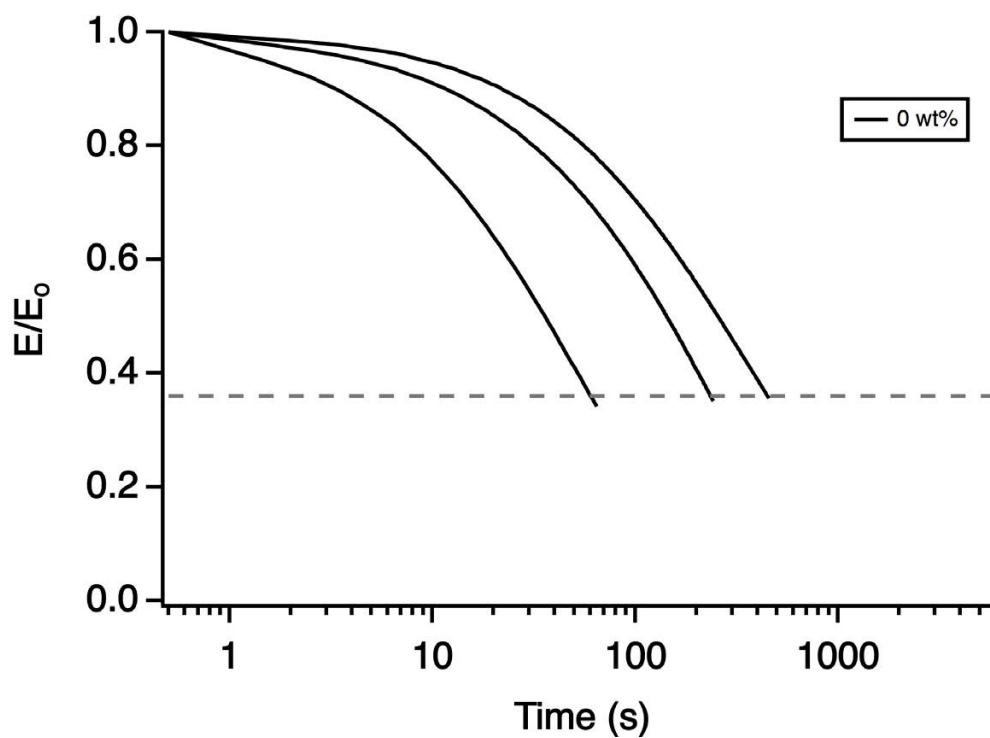
Figure S25. Stress relaxation curves for the 0 wt% film for 160 °C to 180 °C from left to right respectively.
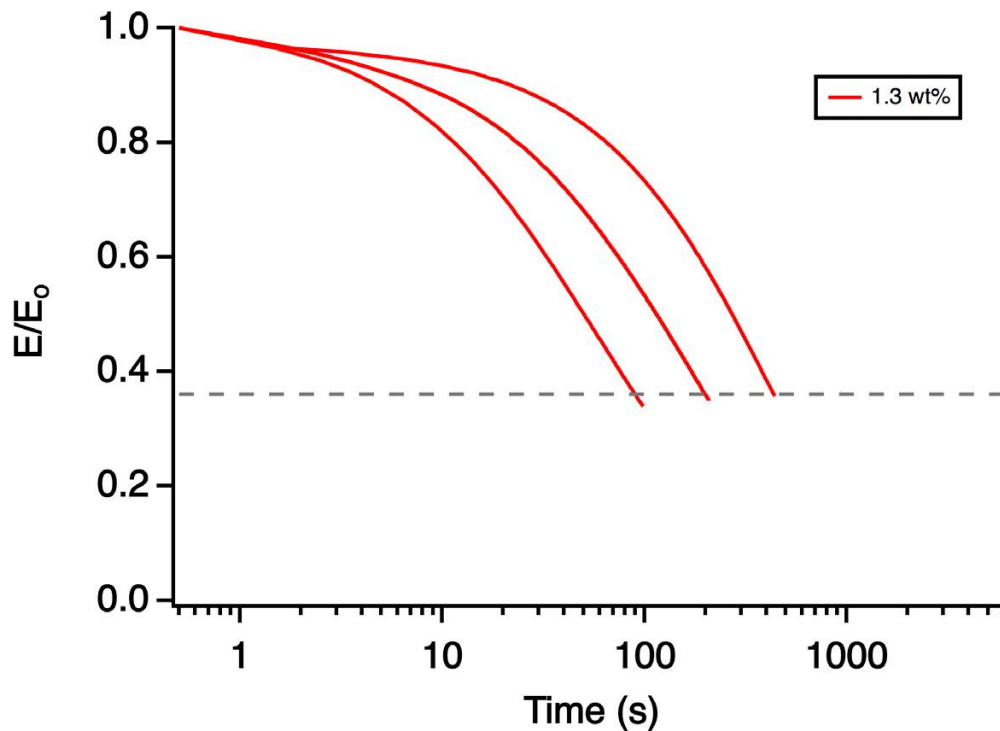
Figure S26. Stress relaxation curves for the 1.3 wt% film for 160 °C to 180 °C from left to right respectively.
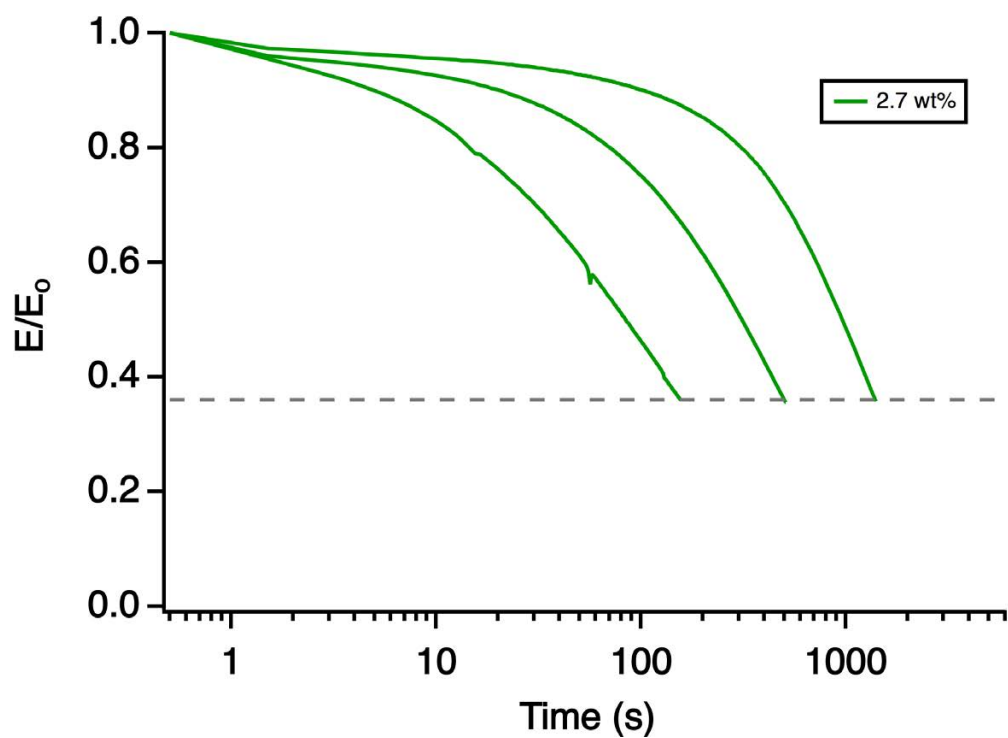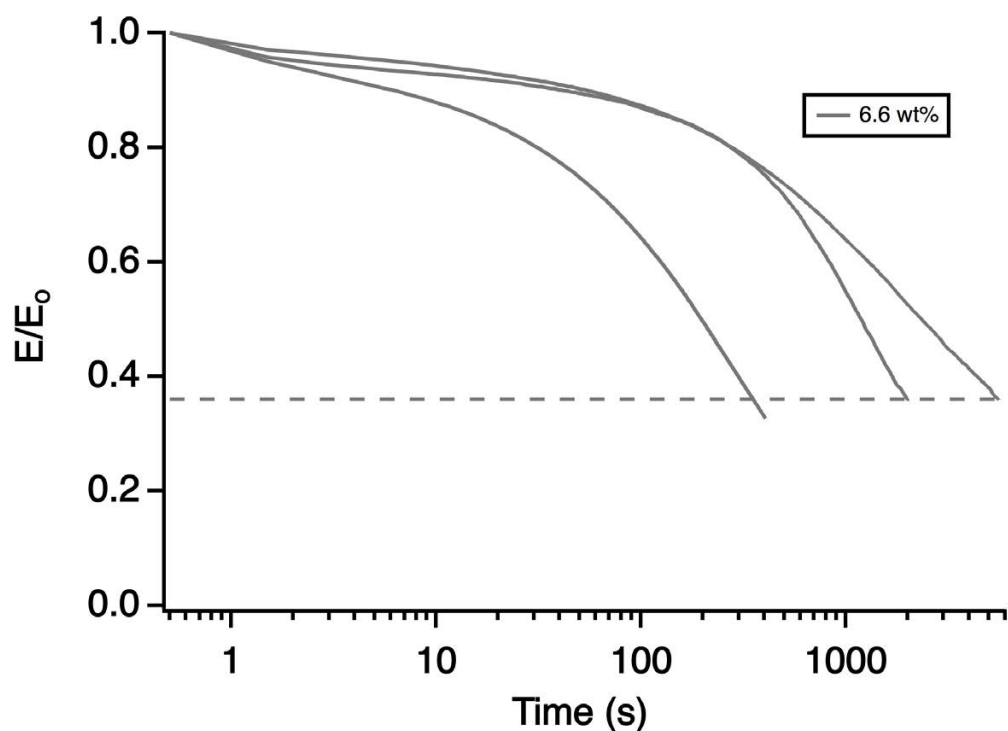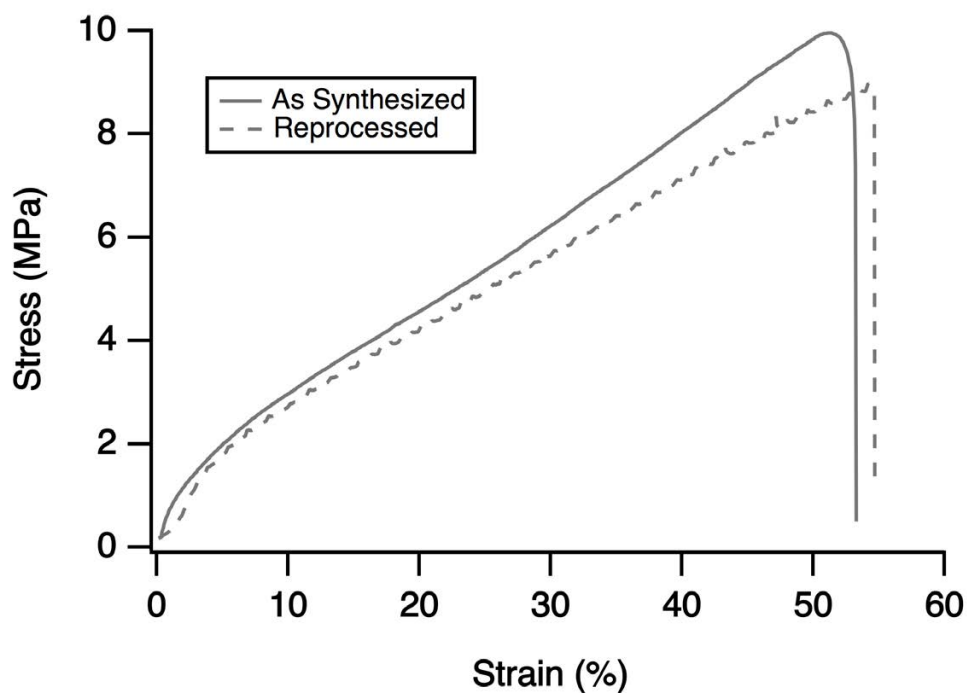
Figure S27. Stress relaxation curves for the 2.7 wt% film for 160 °C to 180 °C from left to right respectively.
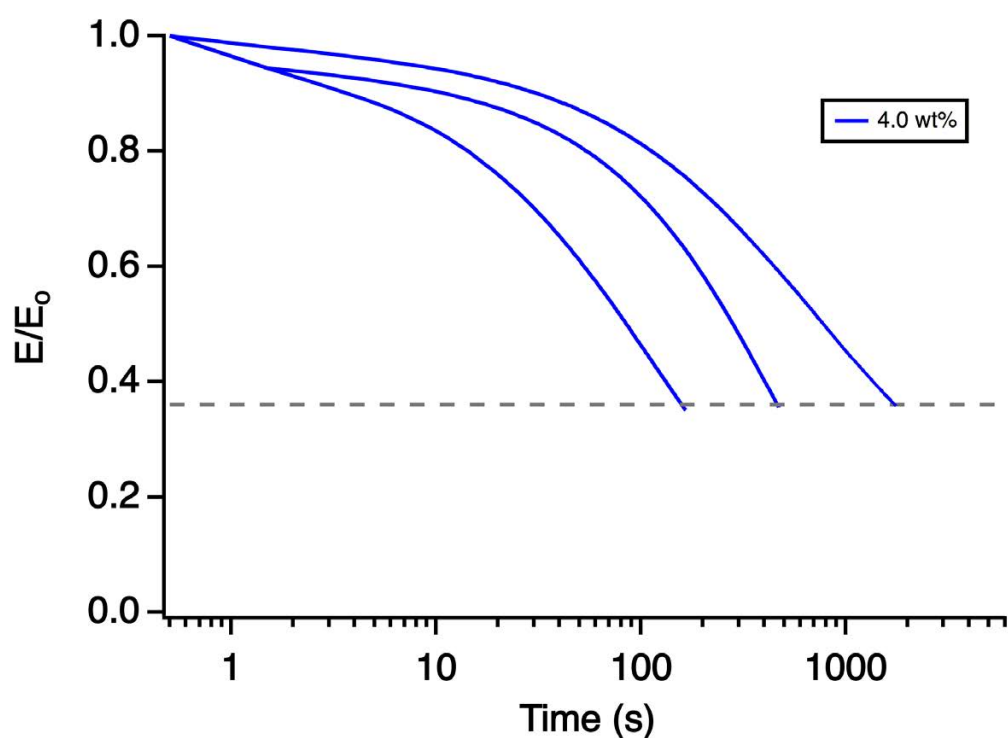
Figure S28. Stress relaxation curves for the 4.0 wt% film for 160 °C to 180 °C from left to right respectively.

S-25
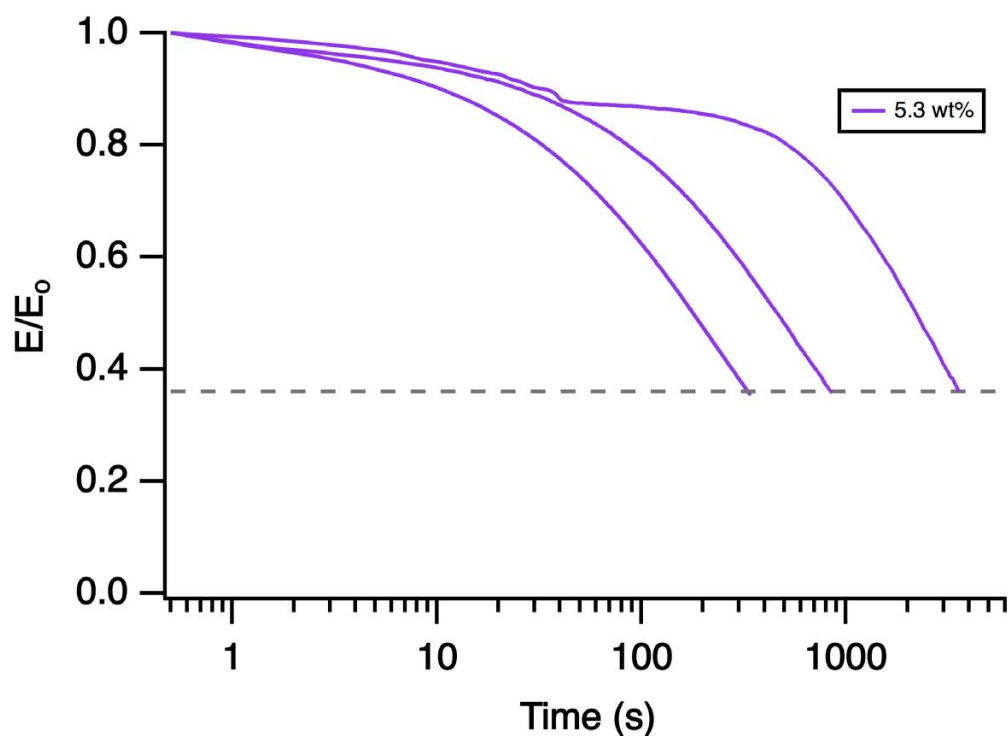
Figure S29. Stress relaxation curves for the 5.3 wt% film for 160 °C to 180 °C from left to right respectively.

Figure S30. Stress relaxation curves for the 6.6 wt% film for 160 °C to 180 °C from left to right respectively.

Polycarbonate Films-Reprocessing Data
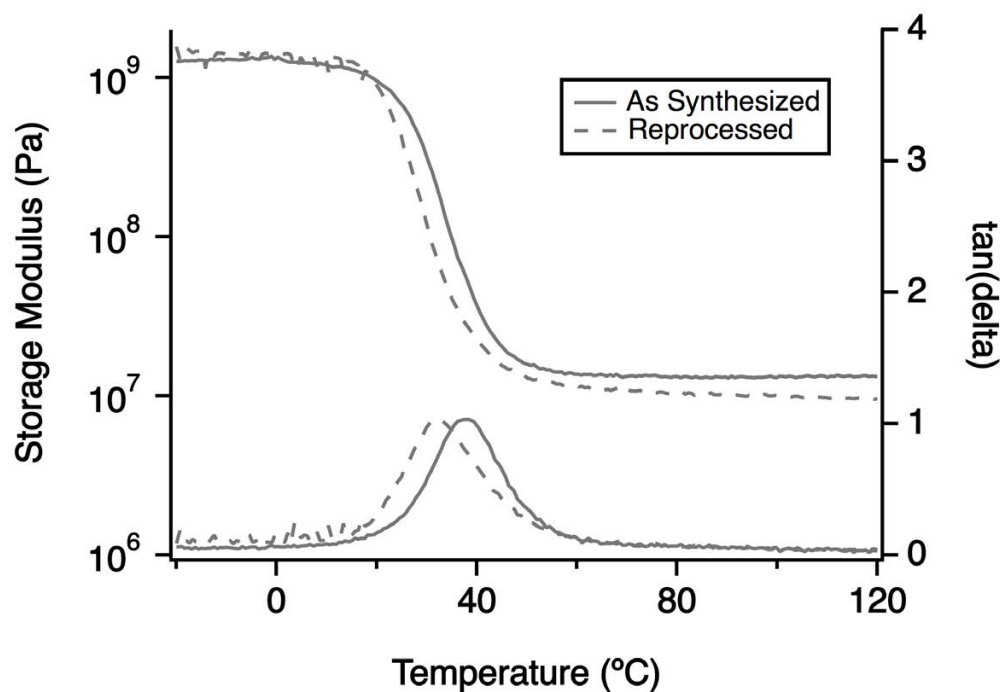
Figure S31. DMTA plot of 6.6 wt% as synthesized and reprocessed showing a decrease in T_g after reprocessing at 140 °C for 8 hours followed by curing for 2 days at 120 °C, resulting in a 75% recovery in crosslink density in the reprocessed sample compared to as synthesized.

Table S8. DMTA data for the reprocessed samples.

Sample	E' at 100 °C (MPa)	M_x (g/mol)	$T_{g,onset}$ (°C)
2.7 wt% 1st Reprocessed	5.25	709	15
2.7 wt% 2nd Reprocessed	4.62	805	19
6.6 wt% 1st Reprocessed	9.90	376	22

Figure S32. Tensile data of 6.6 wt% sample before and after reprocessing showing an 83% recovery in tensile stress compared to as synthesized.

Polyurethane Films-SRA Plots and Data
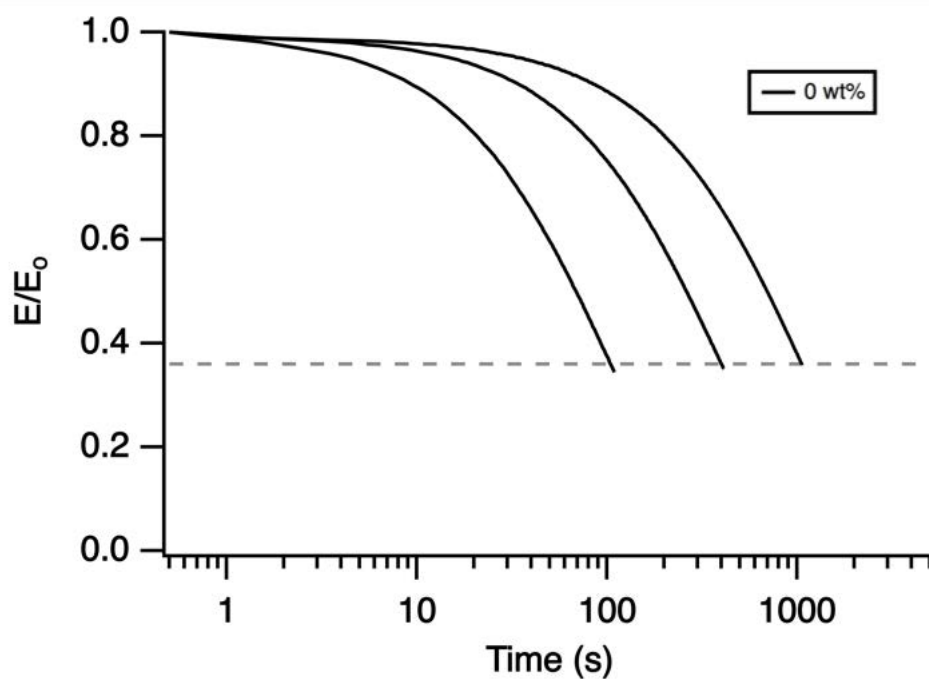
Figure S33. Stress relaxation curves for the 0 wt% film for 140 °C to 120 °C from left to right respectively.
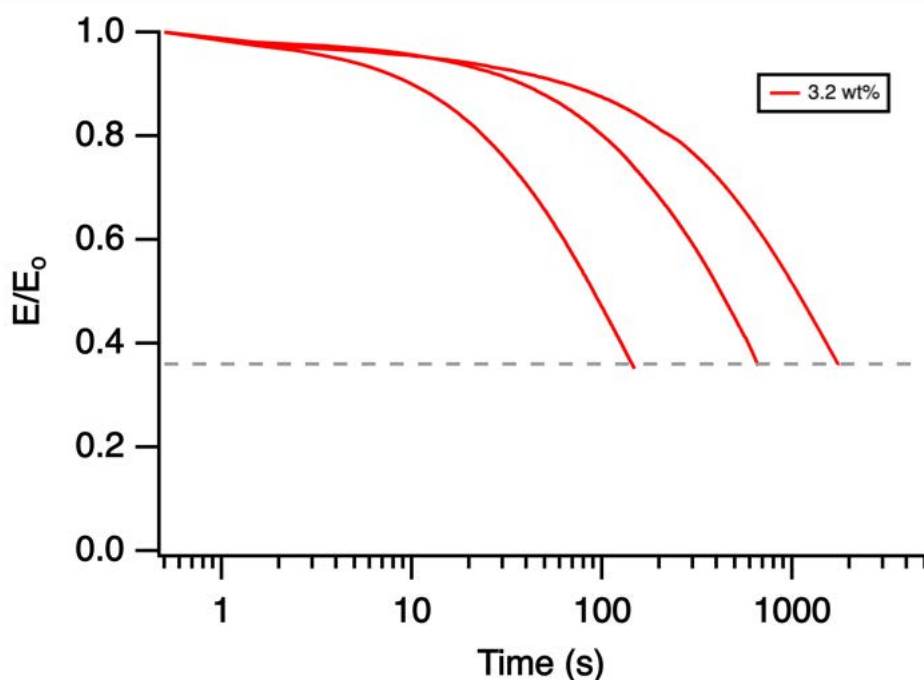
Figure S34. Stress relaxation curves for the 3.2 wt% film for 140 °C to 120 °C from left to right respectively.

Table S9. Relaxation times ($\tau*$) from 120-140 °C for the control and functionalized cellulose-incorporated polyurethane films.

Cellulose Content in Sample (wt%)	120 °C	130 °C	140 °C
0	1327	400	116
	1057	542	104
	912	419	98
3.2	1911	455	190
	1744	472	144
	1670	440	136

Table S10. Examples of mechanical properties of other polycarbonate and polyurethane CANs as a comparison to the cellulose-filled PC and PU CANs.

| Reference	Matrix	Tensile Modulus (GPa)	Tensile Strength (MPa)	Strain at Break (%)	Rigid or Elastomeric
1	Polycarbonate	0.5 ± 0.1	16 ± 1	54 ± 5	Rigid
2	Polyhydroxyurethane	1.9 ± 0.1	34 ± 11	2.0 ± 0.7	Rigid
3	Polyurethane	1.78 ± 0.04	35.8 ± 5.1	2.1 ± 0.4	Rigid
3	Polyurethane	0.002 ± 0.0008	1.10 ± 0.10	61.7 ± 14.0	Elastomeric
4	Polyurethane	1.8 ± 0.2	46 ± 6	3.2 ± 0.9	Rigid
5	Polyurethane	2.86 ± 0.30	3.3 ± 0.3	155 ± 9	Elastomeric

FT-IR Data
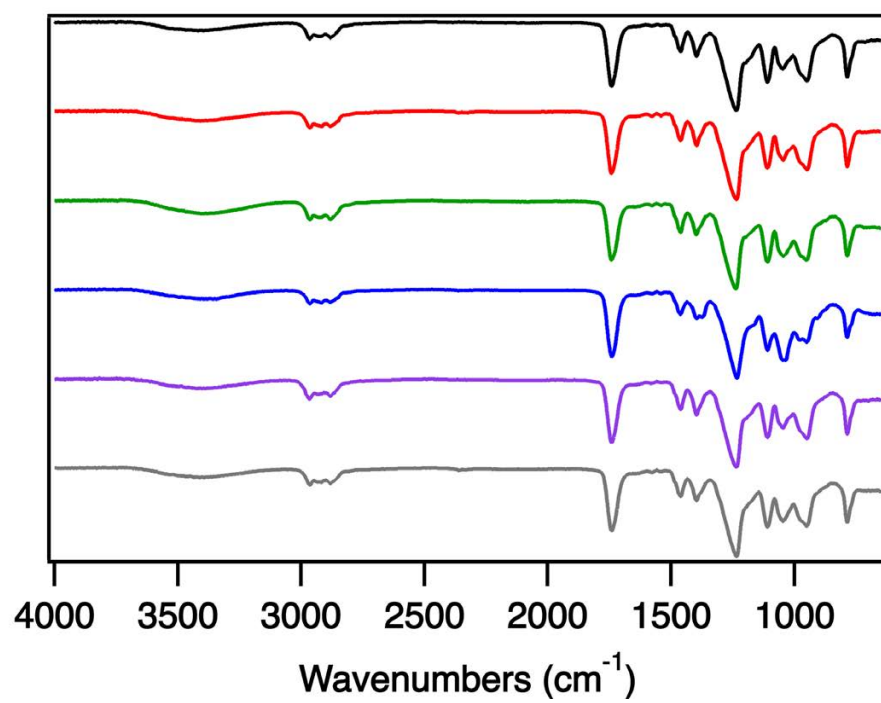
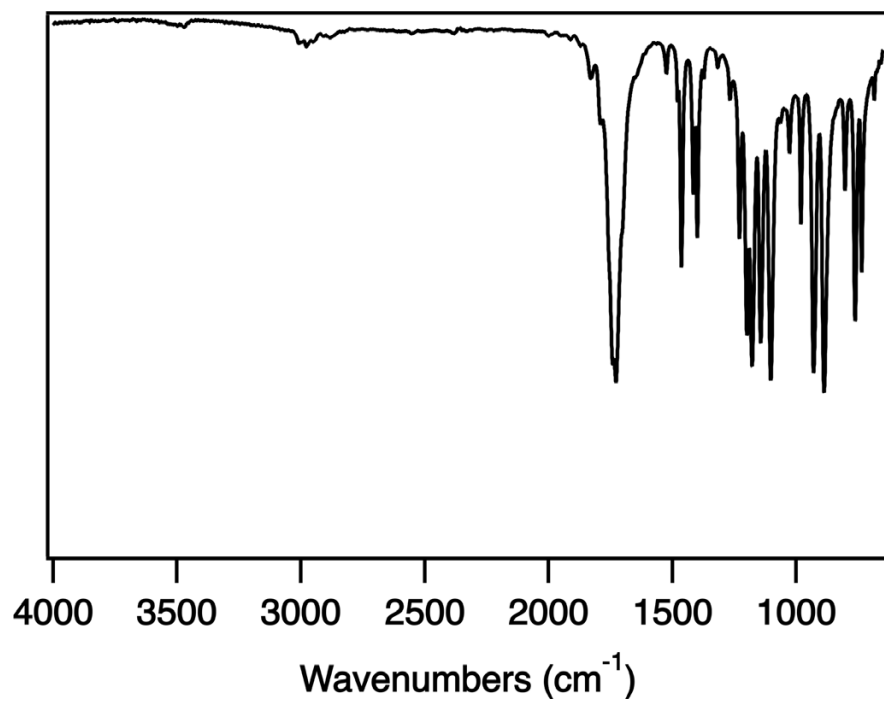**Figure S35.** FTIR of the polycarbonate films once fully cured.
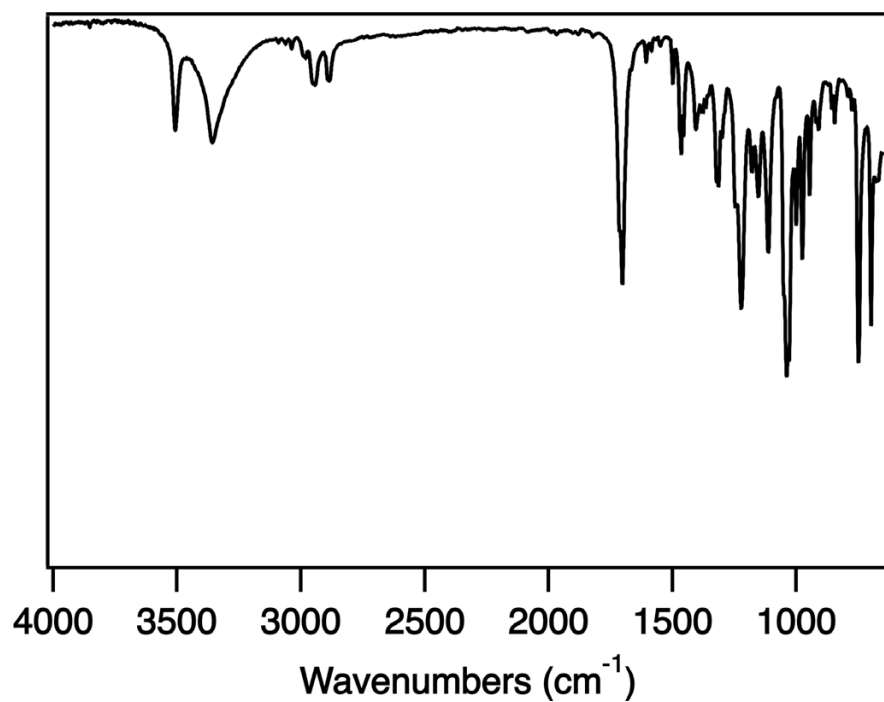
Figure S36. FTIR spectrum of **S1**.
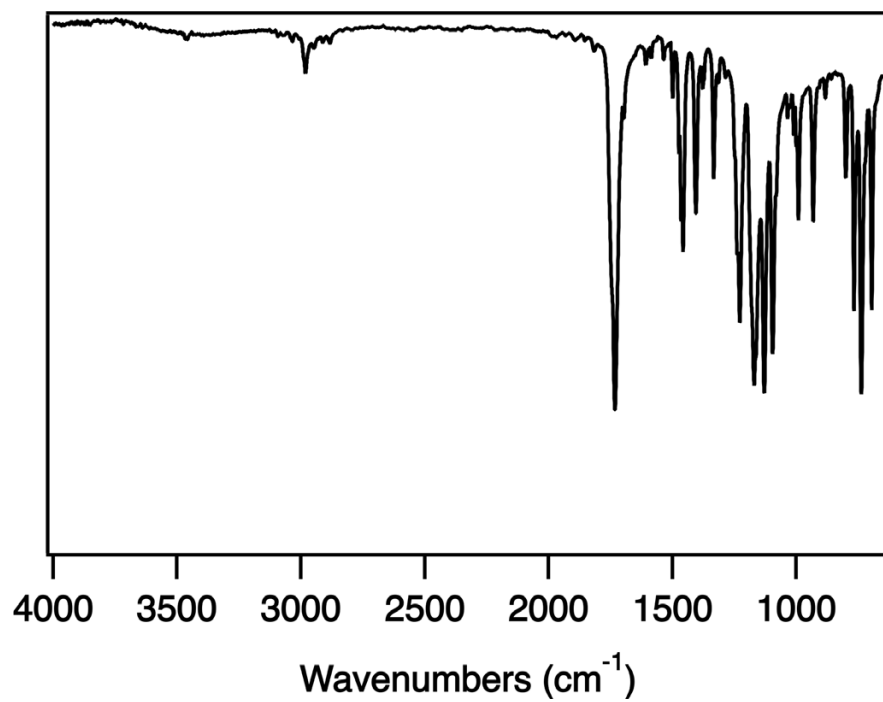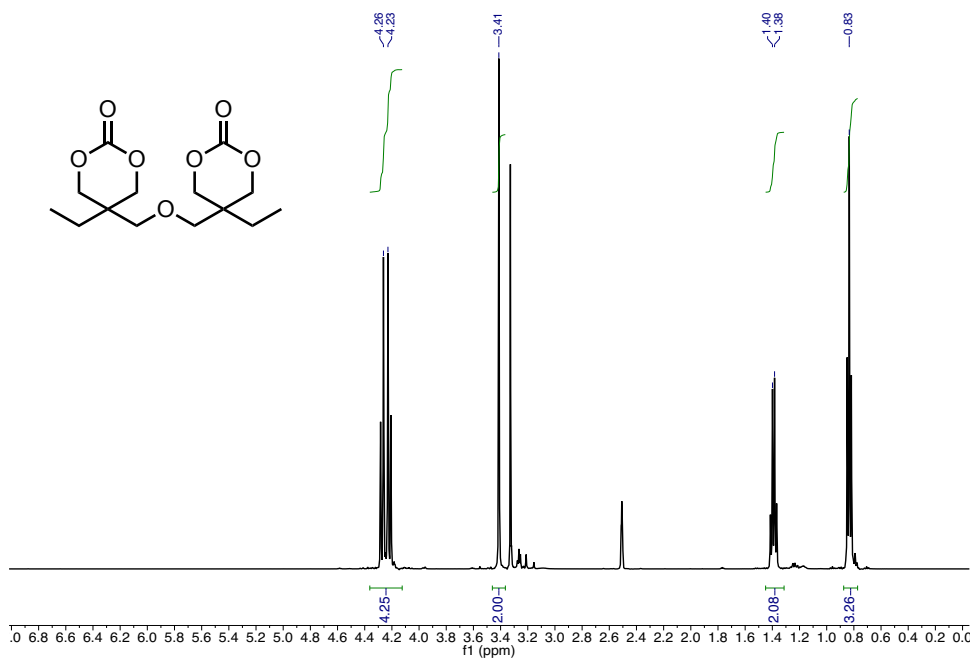
Figure S37. FTIR spectrum of **S2**.
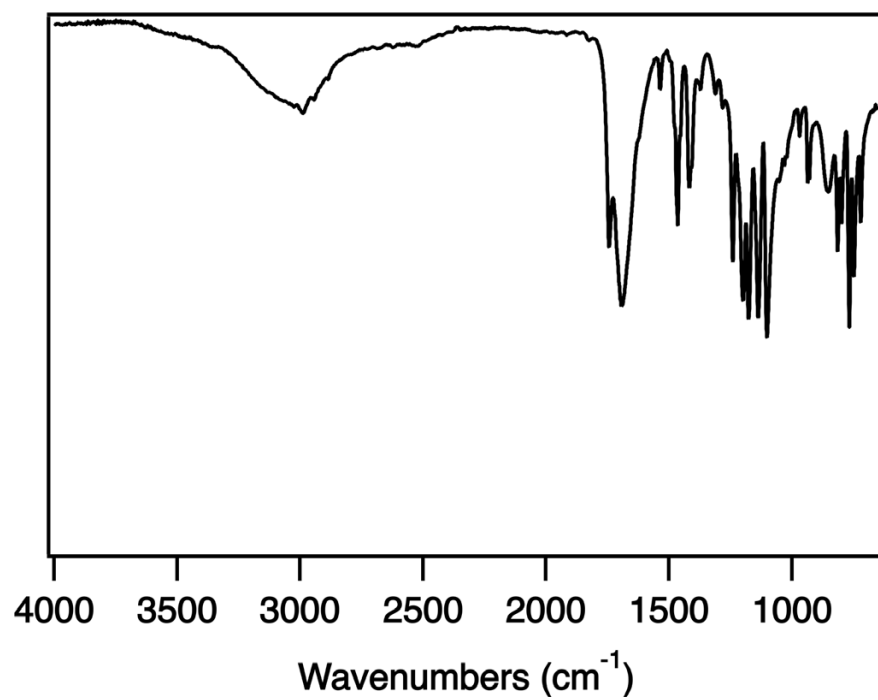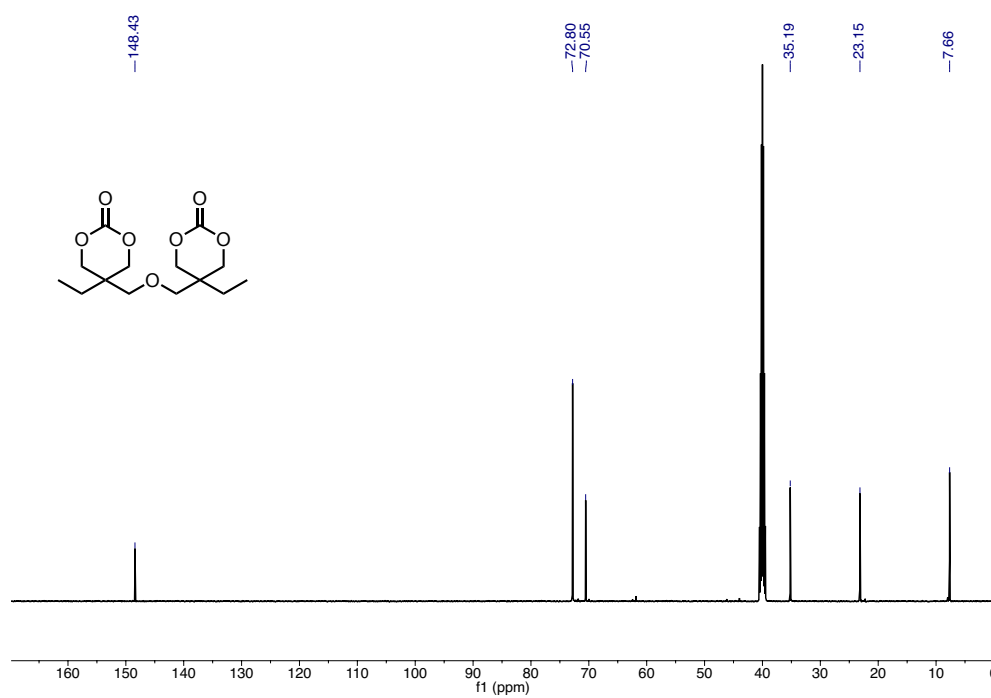

Figure S38. FTIR spectrum of **S3**.
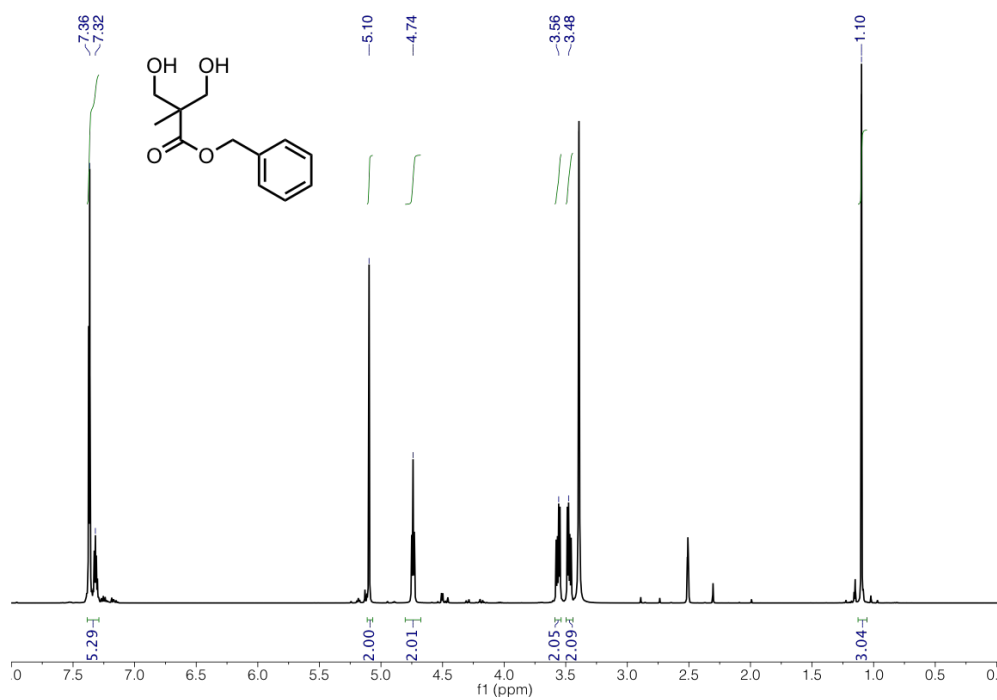
Figure S39. FTIR spectrum of **1**.

NMR Spectra
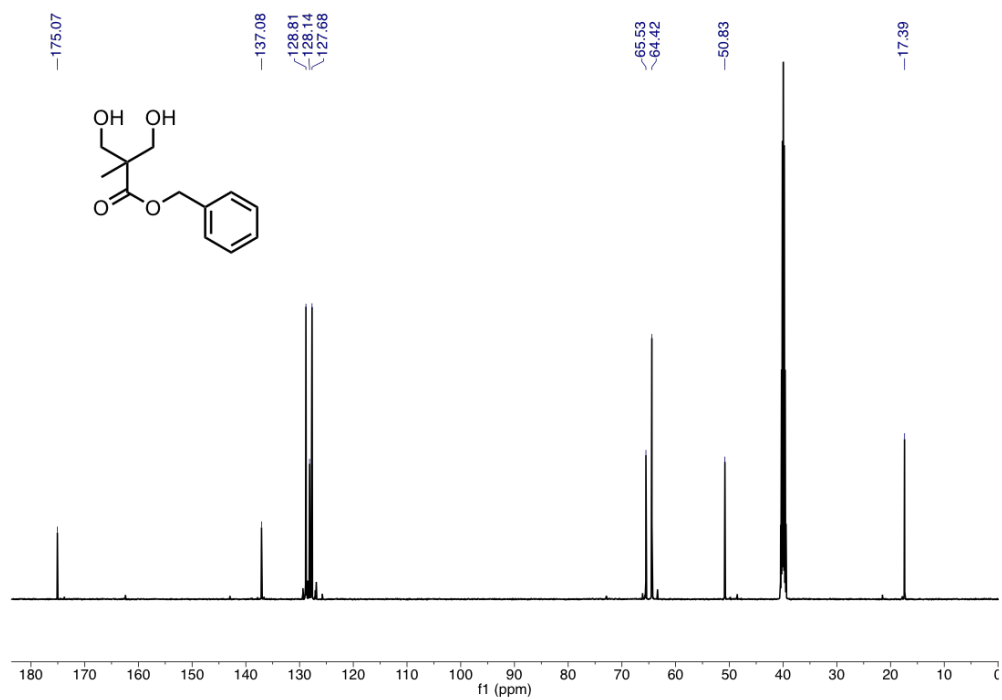

Figure S40. ^{1}H NMR (500 MHz, d_6-DMSO) of **4**.

Figure S41. ^{13}C NMR (125 MHz, d_6-DMSO) of **4**.

Figure S42. ^{1}H NMR (500 MHz, d_6-DMSO) of **S1**.

Figure S43. ^{13}C NMR (125 MHz, d_6-DMSO) of **S1**.
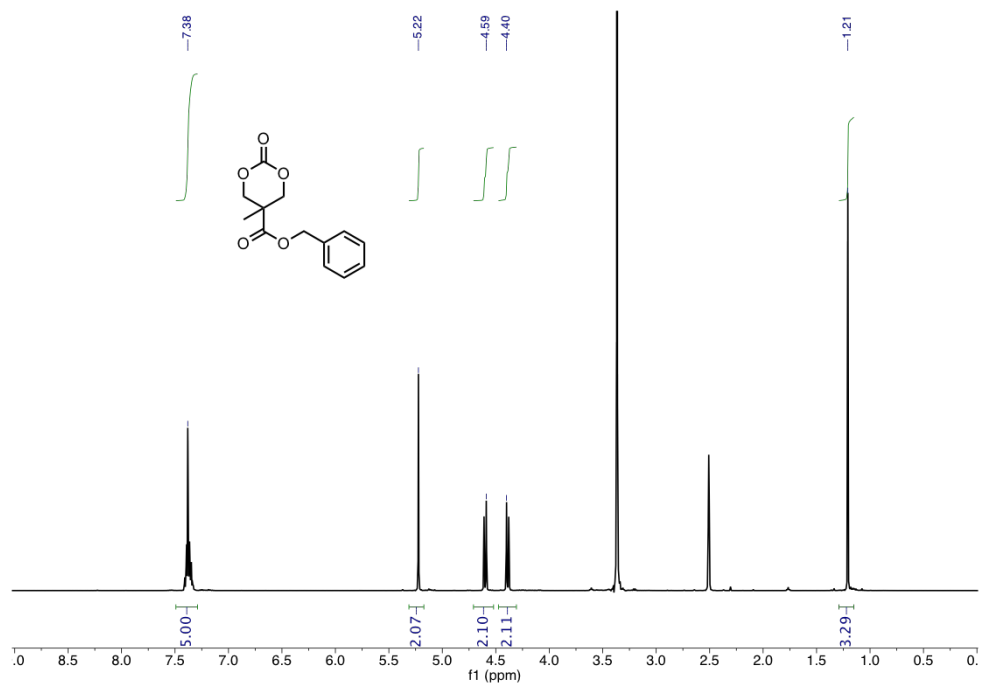
Figure S44. ^{1}H NMR (500 MHz, d_6-DMSO) of **S2**.
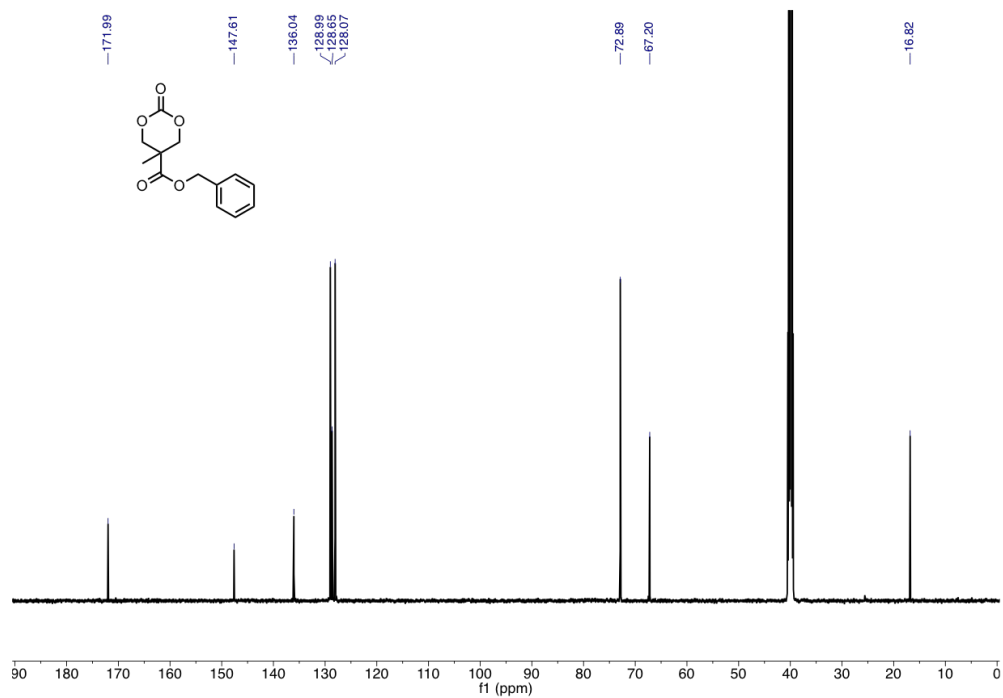
Figure S45. ^{13}C NMR (125 MHz, d_6-DMSO) of **S2**.
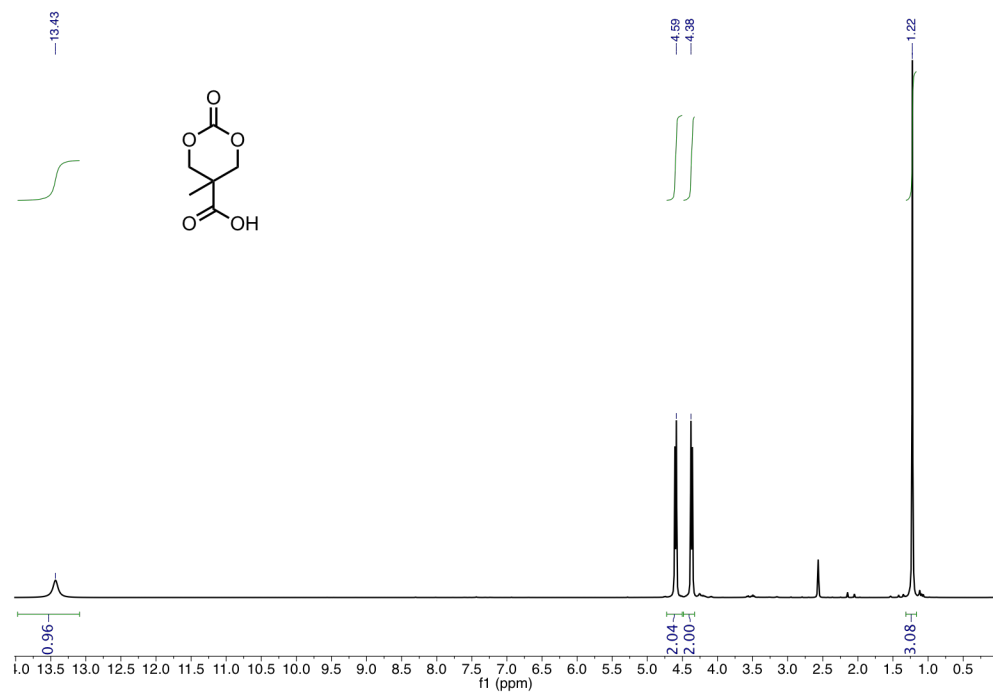
Figure S46. ^{1}H NMR (500 MHz, d_6-DMSO) of **S3**.
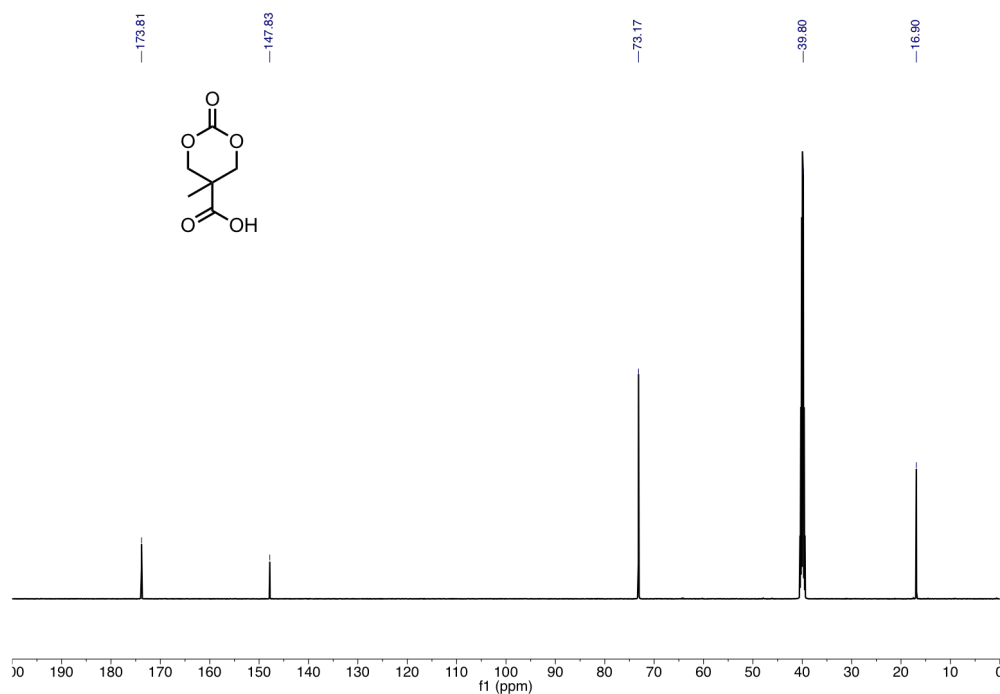
Figure S47. ^{13}C NMR (125 MHz, d_6-DMSO) of **S3**.

References

(1) Snyder, R. L.; Fortman, D. J.; De Hoe, G. X.; Hillmyer, M. A.; Dichtel, W. R. *Macromolecules* **2018**, *51*, 389-397.

(2) Fortman, D. J.; Snyder, R. L.; Sheppard, D. T.; Dichtel, W. R. *ACS Macro Lett.* **2018**, *7*, 1226-1231.

(3) Fortman, D. J.; Sheppard, D. T.; Dichtel, W. R. *Macromolecules* **2019**, *52*, 6330-6335.

(4) Brutman, J. P.; Delgado, P. A.; Hillmyer, M. A. *ACS Macro Lett.* **2014**, *3*, 607-610.

(5) Sheppard, D. T.; Jin, K.; Hamachi, L.; Dean, W.; Fortman, D. J.; Ellison, C. J.; Dichtel, W. R. *ACS Cent. Sci.* **2020**, *6*, 921-927.